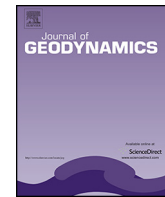




Contents lists available at ScienceDirect

Journal of Geodynamics

journal homepage: <http://www.elsevier.com/locate/jog>



New constraints on the evolution of the Gibraltar Arc from palaeomagnetic data of the Ceuta and Beni Bousera peridotites (Rif, northern Africa)

Thomas Berndt^{a,*}, Vicente Carlos Ruiz-Martínez^a, Ahmed Chalouan^b

^a Departamento de Física de la Tierra, Astronomía y Astrofísica I, Facultad de Ciencias Físicas, Universidad Complutense de Madrid, Avda. Complutense, s/n, 28040 Madrid, Spain

^b Département de Géologie, Faculté des Sciences, BP 1014, Rabat 10000, Morocco

ARTICLE INFO

Article history:

Received 25 February 2014

Received in revised form

29 September 2014

Accepted 30 September 2014

Available online xxx

Keywords:

Palaeomagnetism

Beni Bousera peridotites

Ceuta peridotites

Block rotations

Rif

ABSTRACT

The Betic Cordillera and the Moroccan Rif together form one of the smallest and tightest orogenic arcs on Earth and almost completely close the Mediterranean to the west. For the explanation of the geodynamic evolution of the mountain belt, palaeomagnetic data that generally found clockwise block rotations in the Iberian and anticlockwise rotations in the Moroccan part of the mountain belt, have played a key role in recent works. This palaeomagnetic study has found new constraints on the rotations and timing of the peridotitic bodies outcropping in the key position at the westernmost margin of the mountain belt, in Ceuta and Beni Bousera (Rif, northern Africa).

Detailed thermal demagnetization of 115 individually oriented samples from 14 sites was combined with rock magnetic and scanning electron microscopic experiments to analyze the magnetic mineralogy responsible for the remanences and the mechanisms and relative times of their acquisition. In Ceuta, up to three magnetic components, and in Beni Bousera, up to two magnetic components have been found, that are all to be interpreted as chemical remanent magnetizations (CRM). The data suggests the following succession of geodynamic events affecting the peridotites until recent times: (1) after their exhumation and subsequent cooling about 20 Ma ago, they recorded a characteristic remanent magnetization of both normal and reversed polarities, carried by (pseudo-)single-domain magnetite grains; (2) after their dismembering, the Ceuta peridotites were tilted southward by 22–34° about a horizontal or tilted axis (up to plunge 50°) with an azimuth of 72–145° and the Beni Bousera peridotites were rotated anticlockwise by $72.3 \pm 12.1^\circ$ about a vertical axis and (3) both recorded another magnetic signal of normal polarity only, carried by multi-domain magnetite grains; and finally (4) the Ceuta peridotites rotated anticlockwise by $19.7 \pm 5.9^\circ$ about a vertical axis.

This study provides the first palaeomagnetic data for the Ceuta peridotites that, with their tilt and recent small net rotation, had a distinct geodynamic evolution from the large net rotations about vertical axes in Beni Bousera and Ronda (Betic Cordillera). Moreover, earlier palaeomagnetic data for Beni Bousera is improved, as mixed polarities have been found in the older of the remanences for the first time, and its interpretation as a CRM changes the rotation timing that was proposed previously. The sequence of events exposed in this work are important constraints that need to be incorporated in any geodynamic model of the evolution of the Betic–Rifean mountain belt.

© 2014 Elsevier Ltd. All rights reserved.

1. Introduction

The Betic Cordillera in southern Iberia and the Moroccan Rif together form the northern and southern limbs of the Gibraltar Arc, an arc-shaped mountain belt closing almost completely the Mediterranean to the west. It is one of the tightest orogenic arcs worldwide, and is an example of two opposite processes: mountain building and subsequent collapse. The latter process formed the

* Corresponding author. Present address: Department of Earth Science and Engineering, Royal School of Mines, Imperial College London, Prince Consort Road, SW7 2BP London, United Kingdom. Tel.: +44 7930903913.

E-mail addresses: t.berndt13@imperial.ac.uk (T. Berndt), vcarlos@fis.ucm.es (V.C. Ruiz-Martínez), chalouan@fsr.ac.ma (A. Chalouan).

Alboran Sea in the core of the system while thrusts and folds propagated towards the external zones. The Gibraltar Arc was formed from a geodynamic process which resulted in the consumption of the Ligurian–Maghrebian Tethys and opening of the West Mediterranean Sea (Chalouan et al., 2008; Platt et al., 2013). This evolution started from the Late Eocene and lasted for about 30 million years while the Africa–Europe convergence was going on. In order to explain the evolution of the Betic–Rifean mountain belt, both structural analysis (e.g. Balanyá and Garcí a-Due nas, 1987; Frizon de Lamotte et al., 1991) and palaeomagnetic studies have been undertaken (e.g. Platzman, 1992; Platzman et al., 1993).

Most palaeomagnetic works (see below) indicated large clockwise rotations in the western part of the Betics and anticlockwise rotations in the western Rif that are probably of early Miocene age (Fig. 1(b) shows some of the rotations found). The timing and the exact magnitude of the rotations, however, remains poorly constrained in much of the available data (see Section 1.2).

Various models have been proposed to explain the evolution of the Betic–Rif mountain belt. Amongst them are: Models of a collisional orogeny unrelated to any subduction zone (e.g. Platt and Vissers, 1989); models involving a single, NW-dipping subduction zone (e.g. Lonergan and White, 1997); and models involving two subductions zones, one Cretaceous–Eocene, E-dipping followed by an Oligocene–Neogene, NW-dipping subduction zone with a so-called “Alkapeca” microplate inbetween (e.g. Andrieux et al., 1971; Michard et al., 2002; Chalouan and Michard, 2004). Large block clockwise and anticlockwise rotations in the Betics and the Rif, respectively, favour an interpretation involving a westward slab rollback (Lonergan and White, 1997; Chalouan and Michard, 2004), whilst they do not offer an adequate explanation for deviations from this rotation pattern, such as the clockwise rotations in the Tetuan area in the Rif (Platzman et al., 1993). In any case, any proposed model should explain the observed palaeomagnetic rotations.

In the following, we will present new palaeomagnetic data from the Ceuta peridotites (Sarchal cliffs) in the westernmost part of the Rif and for the Beni Bousera peridotites some 100 km further southeast in the Rif. The Ceuta peridotites have a key position just at the border between the Betics and the Rif and have not been studied palaeomagnetically before. The comparison between the Ceuta and the Beni Bousera peridotites facilitated the interpretation of the palaeomagnetic data from Ceuta which turned out to have had a more complex history than Beni Bousera. By using the same experimental methodology and putting special emphasis on the analysis of the magnetic mineralogy of the two sites, parallels could be drawn that helped constraining the timing of acquisition of the NRM. Moreover, the reliability and accuracy of the palaeomagnetic data of Beni Bousera that was already available (Saddiqi et al., 1995) could be improved by this study, in particular, as both normal and reversed polarity rotated components have been found for the first time.

The obtained experimental data is then used to develop a coherent model that explains successive tectonic stages of the Beni Bousera and Ceuta peridotites during the last 20 Ma.

1.1. Geological setting

The Rif consists of three major domains, as indicated in Fig. 1(a): the *External Zones*, the *Maghrebian Flysch Nappes*, and the *Internal Zones* (Chalouan and Michard, 2004). The Internal Zones consist of three nappe complexes, at the bottom and in the SW the Dorsale Calcaire, then the Ghomaride nappes and at the top and in the NE, the Sebtide nappes (which corresponds to the Alpujarride nappes in the Betics). The Sebtide complex consist of a number of metamorphic units that are deformed by the Beni Bousera and the Beni Mezala antiforms (Michard et al., 1997). From top to bottom theses

units are the Federico units, the Filali schists and gneisses, the Beni Bousera kinzigites and peridotites and finally the Sebta gneisses (see Fig. 1(c) and (e)).

The Beni Bousera peridotites crop out 60 km SE of Tetuan, over an area of about 75 km². It is an antiform with NW–SE oriented fold axis and the peridotites are mainly spinel lherzolites and harzburgites (Fig. 1(e)). Moreover, minor amounts of dunite are present, and bands of pyroxenite constitute up to 5–10% of the massif (Kornprobst, 1969).

In the Sarchal cliffs in Ceuta, peridotites crop out over an area of a few hectares (see Fig. 1(d)). It is situated between granulitic gneisses and a porfidic gneissic granitoid. The Ceuta peridotites form part of a more or less continuous thin peridotitic layer that also crops out in Beni Bousera (Sánchez-Gómez et al., 1995).

1.2. Former palaeomagnetic studies of the Betic–Rif

Various palaeomagnetic studies have investigated the Betic–Rifean mountain chain and generally found a pattern of clockwise block rotations in the Betics and anticlockwise rotations in the Rif. Early palaeomagnetic studies involved mainly Jurassic and Cretaceous sedimentary rocks in the External Betics (Platzman, 1992; Platzman and Lowrie, 1992; Osete et al., 1988, 1989; Allerton et al., 1993), where generally clockwise block rotations in the range of 40–70° were found, and in the Internal Rif (Platzman, 1992; Platzman et al., 1993), where generally anticlockwise rotations in the range of 60–100° were found. One notable exception were a few sites near Tetuan (Morocco), where Platzman et al. (1993) found significant clockwise rotations, although the reliability of this result can be questioned, due to its large error and/or strong tilt of the bedding. These studies interpreted the magnetic components they found to be primary natural remanent magnetizations (NRM) and hence of Mesozoic age.

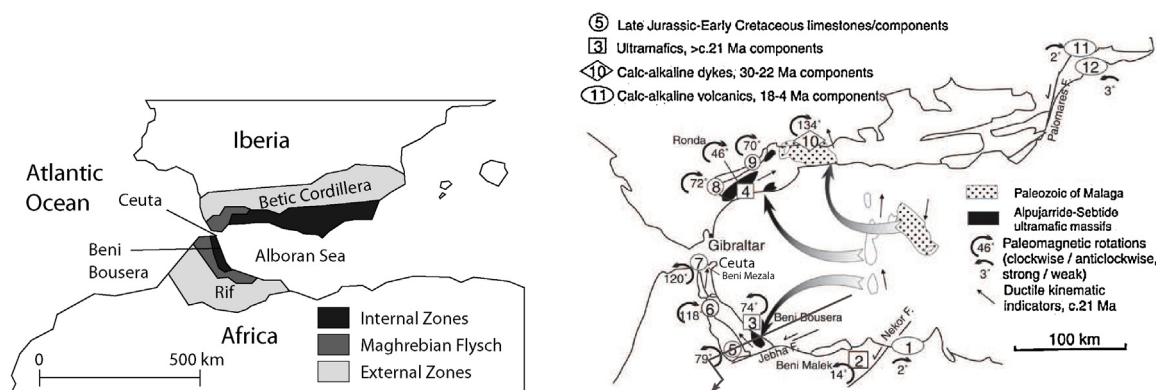
Villaláin et al. (1996), however, suggested that some of these components may indeed be younger remagnetizations, possibly of Neogene age. Misinterpreting a remagnetization as a primary NRM would not only change the timing constraints of these rotations, but also decrease (increase) the amounts of clockwise (anticlockwise) block rotations by as much as 35°, as the Mesozoic expected direction for stable Iberia and stable Northwest Africa was rotated westward compared to the Neogene expected direction. Other studies (Villaláin et al., 1994; Saddiqi et al., 1995; Villaláin et al., 1996; Feinberg et al., 1996; Calvo et al., 2001; Villasante-Marcos et al., 2003; Mattei et al., 2006; Cifelli et al., 2008) found direct evidence of Neogene block rotations of the same pattern (clockwise in the Betics, anticlockwise in the Rif).

On the other hand, some studies show evidence that rotations were already completed by Neogene times, such as Osete et al. (2004) who found a rotated (clockwise, 35–140°) primary NRM on Mesozoic rocks from the Betics and an almost non-rotated Neogene remagnetization. Also, some studies on Neogene rocks (Calvo et al., 1997; Krijgsman and Garcés, 2004) showed no rotations. Various studies conclude that there are no significant block rotations further East of the Betic–Rifean mountain chain (Calvo et al., 1994, 1997; Najid et al., 1981) since the Miocene.

1.3. Former studies of the Beni Bousera/Ronda peridotites

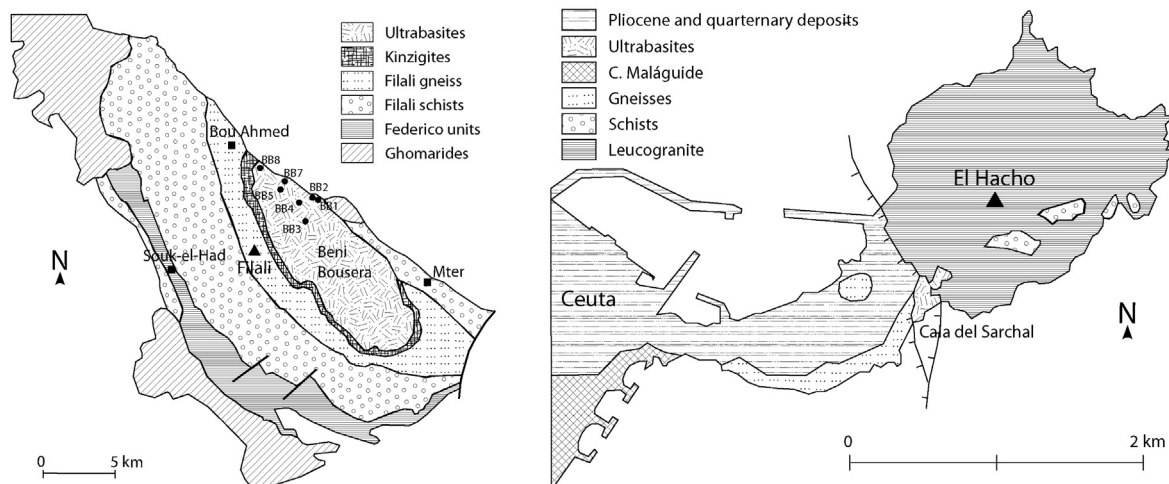
1.3.1. Thermal evolution

Various studies have investigated the exhumation of the Betics (for example Monié et al. (1991), Zeck et al. (1992), Sánchez-Rodríguez and Gebauer (2000)) and the Rif (Beni Bousera, for example Loomis (1975), Seidemann (1976), Michard et al. (1983), Afiri et al. (2011)). They all gave similar ages in the range 19–24 Ma



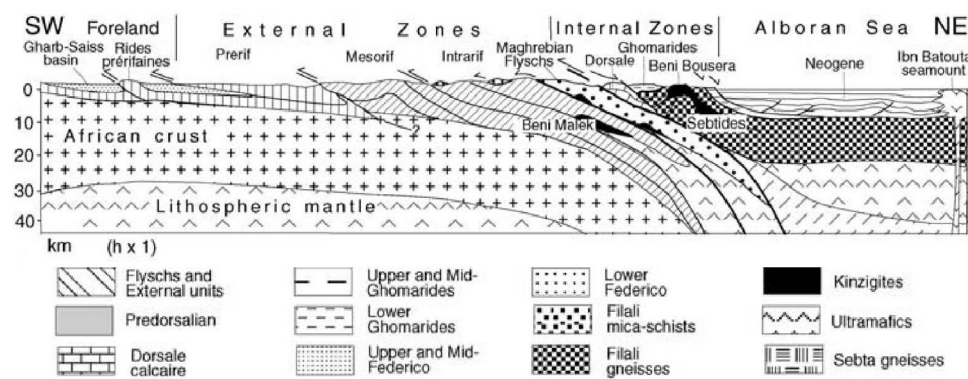
(a) Geological map of the Alboran domain. After Gysi et al. (2011).

(b) Palaeomagnetic rotations in the Betic-Rif mountain belt after Chalouan and Michard (2004) and Feinberg et al. (1996). Grey line indicates cross-section in Fig. 1e.



(c) Geological map of Beni Bousera with sampling sites indicated. After Saddiqi et al. (1995); Michard et al. (1997); Chalouan and Michard (2004).

(d) Geological map of Ceuta. After Sánchez-Gómez et al. (1995).



(e) Cross-section of the Beni Bousera anticline as indicated by the grey line in Fig. 1b (Chalouan and Michard, 2004).

Fig. 1. Geological setting. (a) Geological map of the Alboran domain. After [Gysi et al. \(2011\)](#). (b) Palaeomagnetic rotations in the Betic–Rif mountain belt after [Chalouan and Michard \(2004\)](#) and [Feinberg et al. \(1996\)](#). Grey line indicates cross-section in (e). (c) Geological map of Beni Bousera with sampling sites indicated. After [Saddiqi et al. \(1995\)](#), [Michard et al. \(1997\)](#), [Chalouan and Michard \(2004\)](#). (d) Geological map of Ceuta. After [Sánchez-Gómez et al. \(1995\)](#). (e) Cross-section of the Beni Bousera anticline as indicated by the grey line in (b) ([Chalouan and Michard, 2004](#)).

for the last high temperature metamorphism in the crustal rocks surrounding the peridotites and granitoid dykes.

Sánchez-Rodríguez and Gebauer (2000), in particular, investigated zircons of eclogite-bearing magmatites overlying the Ronda peridotites in southern Spain and anatetic granites crosscutting both the peridotites and the country rocks. They established a peak temperature of 790 ± 15 °C of high pressure/high-temperature metamorphism of the country rocks that is dated at 19.9 ± 1.7 Ma, followed by a rapid exhumation of >31 mm/y with a decompression from 17 ± 1 kbar to less than 8 kbar and then a rapid cooling of 200–340 °C/Ma. The granites crystallized at 18.9 ± 3.0 Ma which represents an estimate for the time of emplacement of the peridotites into the middle crust.

According to Villasante-Marcos et al. (2003, and references therein), the post-metamorphic cooling gave rise to the serpentinization and the generation of a first population of sub-microscopic magnetite, until about 17–18 Ma ago ("first serpentinization phase"). Later, up to millimetre-sized magnetite grains formed, mainly along fractures and joints. This "posterior serpentinization phase" started with the extensional dismembering of the peridotite slab. For oceanic peridotites, Maffione et al. (2014) also found a sequence of serpentinization forming smaller magnetite grains in the early stages, and larger grains along fractures at later stages.

The thermal evolution of the Gibraltar Arc is critical for our paleomagnetic study, as magnetic minerals cannot retain any magnetization above a critical temperature (T_C or Curie temperature; e.g., 580 °C for pure, fine magnetite grains; Dunlop and Özdemir, 2009). Although exhumation of the Beni Bousera peridotites took place during the Oligocene–Miocene, P - T data shows that deformation (folded pyroxenite layers, development of the main foliation) occurred during decompression from 1050 °C to 800 °C (Afifi et al., 2011), dated at 25–20 Ma. Therefore, peridotite rocks from the Gibraltar Arc cannot have preserved any information of the geomagnetic field before the above mentioned high temperature event 19–24 Ma ago, but only after they cooled below their Curie temperatures. This implies that the time of any acquisition remanences is younger than the age of formation of their observed deformation pattern.

1.3.2. Palaeomagnetic studies in the Rifian peridotites

Saddiqi et al. (1995) studied 224 oriented samples (11 sites) from the Beni Bousera peridotites and found two stable components carried by magnetite and some hematite. A low-temperature (LT) component with unblocking temperatures between 450 °C and 550 °C had a northward direction ($D = 1.2^\circ$, $I = 57.4^\circ$, $\alpha_{95} = 5.4^\circ$, without tectonic correction). A second, high-temperature (HT) component with unblocking temperatures between 580 °C and 650 °C was found in 6 sites (38 samples) and had an eastward mean direction and reversed polarity ($D = 103.8^\circ$, $I = -58.6^\circ$, $\alpha_{95} = 10.3^\circ$, $k = 43$, without tectonic correction) that is due to the high temperature conditions 22 Ma ago. Saddiqi et al. (1995) interpret the northward LT component as a post-metamorphic TRM that was acquired during the same thermal event and reject the possibility of a chemical remanent magnetization (CRM) for the high unblocking temperature and the results of their ARM experiments that indicated a single size of the magnetic grains. They therefore conclude that an anti-clockwise rotation of the Beni Bousera peridotites of $76 \pm 13^\circ$ took place during the post-metamorphic cooling and was completed by 16 Ma.

1.3.3. Palaeomagnetic studies in the Betic peridotites

Feinberg et al. (1996) studied 11 sites in the Ronda peridotites (Sierra Bermeja and Sierra Alpujata) in the Betic Cordillera, and four granitic dykes intruding them. They performed various rock magnetic experiments and conclude that the main magnetic carrier is

coarse-grained magnetite and in a few samples a small quantity of hematite. About 62% of the samples had a NE normal polarity magnetic component that was either stable up to 600 °C or stable up to 550 °C and then reversed at higher temperatures to a SW reversed polarity direction. In some cases only a reversed polarity component was observed that corresponded in direction to the SW high temperature component. After taking antipodes of the reversed polarity directions, they obtained a mean direction of $D = 46^\circ$, $I = 47.5^\circ$, $\alpha_{95} = 6.6^\circ$, $N = 19$ (without tectonic correction). They also found a present-day field direction that was stable up to 250 °C in some samples. Hence, they conclude that the Ronda massifs acquired their characteristic remanent magnetization (ChRM) during the post-metamorphic cooling, then registered a magnetic field reversal and then rotated $46 \pm 8^\circ$ clockwise before the cooling had completely ended. They hence interpret, like Saddiqi et al. (1995) in Beni Bousera, the components as pure thermoremanent magnetizations and they pinpoint the time of acquisition to the 20–19 Ma period of dominantly normal polarity magnetic field.

Villasante-Marcos et al. (2003) demagnetized 253 oriented samples from the Ronda peridotites (Ronda, Ojén and Carratraca massifs), mainly by thermal demagnetization and in part by AF. They generally cleaned the samples of a magnetic component with a blocking temperature below 200 °C that they interpret as a viscous remanent magnetization (VRM). After cleaning the VRM, samples showed either only a present-day field direction (20% of the samples), or single rotated direction of either polarity (45%), or a low-temperature northward direction followed by a distinct high-temperature component (20%), or had an anomalous behaviour (15%). The rotated component has a mean direction of $D = 45.3^\circ$, $I = 45.8^\circ$, $\alpha_{95} = 7.6^\circ$, $k = 20.4$ (without tectonic correction), which amounts to a $41 \pm 12^\circ$ clockwise rotation when compared to expected palaeodirection for stable Iberia after Barberá et al. (1996).

Although the directions they found, are similar to those obtained by Feinberg et al. (1996), they disagree with them in terms of the mechanism and timing of the acquisition of the NRM: (1) they interpret the northward direction as a post-rotation VRM associated with multi-domain (MD) magnetite grains, as opposed to a TRM and (2) they consider the rotated directions a thermo-chemical remanent magnetization due to the formation of single-domain (SD) or pseudo-single-domain (PSD) magnetite grains. These SD/PSD grains formed during the post-metamorphic cooling when the massif cooled from 350 °C to 400 °C to ambient temperatures, between 20 and 17–18 Ma ago. This hypothesis is supported by the observation that serpentinites carried mostly present-day field directions, whereas peridotites more frequently showed rotated components, and in cases where both components were visible, the northward component was more predominant in the serpentinized samples (assuming that the degree of serpentinization is mainly due to the posterior serpentinization phase).

2. Sampling strategy

Sampling has been performed following standard practices in palaeomagnetism. In total 60 oriented samples have been obtained from Beni Bousera (BB) and 55 from Ceuta (SA, Sarchal cliffs, south-east edge of Monte Hacho). Seven sites per locality (BB and SA, positions are indicated in Fig. 1(c) and listed in Table 1) have been used to average out adequately the secular variation of the terrestrial magnetic field, which makes an average of ca. 9 (BB) and 8 (SA) samples per site, respectively. In the case of Ceuta, it must be noted that the outcrop was very small, only a few hundreds of metres in length along the cliffs of the Sarchal beach. Sampling sites in SA have been separated as far as possible (i.e. a few tens of metres), using the whole width of the outcrop available. Three of them were above sea level during low tide only, the others were always above

Table 1

Coordinates of sampling sites. Note that in the Sarchal cliffs (SA) the sites were only separated by a few tens of metres, therefore only one position is given.

Site	Latitude	Longitude
BB1	35° 18.150'	-4° 53.200'
BB2	35° 18.099'	-4° 53.098'
BB3	35° 17.237'	-4° 53.550'
BB4	35° 18.177'	-4° 54.609'
BB5	35° 15.869'	-4° 55.180'
BB7	35° 18.409'	-4° 54.519'
BB8	35° 18.888'	-4° 55.489'
SA	35° 53.373'	5° 17.750'

sea level. In Beni Bousera, the seven sites were further apart, on average separated a few hundreds of metres to about 2 km.

All the three previous paleomagnetic studies in Ronda and BB (Saddiqi et al., 1995; Feinberg et al., 1996; Villasante-Marcos et al., 2003) used only “in situ” directions (i.e. without tectonic correction), because for all the observed directional components, the fold tests were negative (i.e. tectonically corrected paleomagnetic directions were more scattered than in situ directions), thus indicating that remanence acquisition postdate the deformation. These negative fold tests were performed in BB using the widespread antiformal foliation (Saddiqi et al., 1995) or in Ronda using foliation planes and the compositional layering (Villasante-Marcos et al., 2003). In BB, the results by Saddiqi et al. (1995) results imply that the age of the older remanence is younger than the formation of the NW–SE trending anticline. Taking into account these previous results, foliation/compositional layering planes were measured only at 4 sites from BB and SA in this study. Measured dip direction/dip mean values of foliation planes were: 345/42 (SA1), 323/43 (SA2), 327/53 (BB5), 63/66 (BB8).

In Beni Bousera (BB), sampled peridotites correspond mostly to the spinel Iherzolite facies that crop out in the core of the massif, generally foliated and variably serpentinized, which grade to garnet/spinel Iherzolite/harzburgite in the rim of the massif (BB8 in Fig. 1(c)), where it is generally more foliated (e.g. Reuber et al., 1982; Afifi et al., 2011). The serpentinized peridotites from Ceuta (SA) are foliated and highly tectonized (Sánchez-Gómez et al., 1995).

Palaeomagnetic sampling strategy avoided drilling highly serpentinized bands when detectable at a centimetric scale. Despite of this, we observed a high variability of the degree of serpentinization between individually oriented samples, in fact sometimes between different specimens ($\sim 10 \text{ cm}^3$ each). The degree of serpentinization was measured in representative samples for each site (Martín-Hernández et al., 2009), obtaining mean values of 68.0% (SA) and 62.8% (BB) and a high variability both between and within sites. Samples for those sites with minimum/maximum values of the degree of serpentinization in each locality were selected for SEM analysis (see Section 4).

3. Experimental methods

3.1. Thermal demagnetization

One to two samples of most sites have been taken as *pilot samples* and thermally demagnetized with a Schonstedt TSD-1 furnace with 18 temperature steps from 100 °C to 675 °C. The remaining (“non-pilot”) samples have been thermally demagnetized using a Magnetic Measurements MMTD-80 furnace with much smaller temperature steps. All samples have been demagnetized with temperature steps of 40 °C from 100 °C to 460 °C. After that, smaller temperature steps between 10 °C and 30 °C were used, up to a temperature of 620 °C (SA) and 680 °C (BB) when the samples were completely demagnetized. As both furnaces are known to have a

temperature gradient, the samples have always been placed at the same positions, so that relative temperature steps are accurate.

The remanent magnetization has been measured with an Agico JR5-A spinner magnetometer inside a Helmholtz coil cage. Samples were kept in a magnetic shield most of the time when no measurement was being done with them. All samples have been measured in four positions.

Before beginning the thermal demagnetization, and after every second demagnetization step, the bulk magnetic susceptibility of each sample was measured using an Agico Kappabridge KLY-4S.

3.2. Alternating field demagnetization

A total of 14 specimens of BB and 15 specimens of SA have been demagnetized by alternating fields (AF) using a 2G superconducting magnetometer in steps of 3 mT up to 15 mT and then with steps of 5 mT. Due to instrumental biases at higher fields, measurements above 30 mT had to be discarded. Specimens of four samples have been demagnetized by alternating field demagnetization using a Schonstedt GSD-5 demagnetizer. The sample BB7-6A has first been partially thermally demagnetized up to a temperature of 340 °C and then further AF demagnetized. The other three specimens have been completely AF demagnetized.

3.3. Scanning electron microscope

A few selected samples have been investigated in a JSM-6400 scanning electron microscope (SEM) in the *Centro de Apoyo en Investigación (CAI) for Microscopy* in the Chemistry Faculty of the UCM. Samples have been coated with graphite or gold in order to improve conductance. Moreover, the elementary compositions of different grains of these samples have been measured using energy-dispersive X-ray spectroscopy (EDX).

3.4. Rock magnetic experiments

Isothermal remanent magnetization (IRM) acquisition curves, backfield curves, hysteresis cycles and thermomagnetic (Curie) curves have been obtained from selected samples using a Magnetic Measurements Variable Field Translation Balance (VFTB) in the *CAI for Palaeomagnetism* in the Physics Faculty of the UCM. On some additional samples, hysteresis loops have been obtained using a coercivity metre (Jasonov et al., 1998). Specimens of the same samples investigated in the SEM/EDX have been used to obtain low-temperature thermomagnetic curves using a Quantum Design MPMS-XL SQUID magnetometer in the *CAI Técnicas Físicas* at the Physics Faculty of the UCM.

4. Rock magnetic and SEM results

4.1. Scanning electron microscope results

Fig. 2 shows a representative image obtained by scanning electron microscopy (SEM). Two samples from BB and two from SA have been investigated in a SEM. On these samples, 30 grains have been analyzed using energy-dispersive x-ray (EDX) to obtain their chemical compositions. Table 8 in Appendix lists the atomic percentages of the elements detected by the EDX for the different grains, along with a very rough estimate of the size of the respective grain and a possible interpretation in terms of minerals. This way, the following minerals have been identified: olivine (fayalite/forsterite), pyroxene, pentlandite, iron-oxides (magnetite/hematite/wüstite), chromites and some grains containing copper-oxides. These identifications are listed in Table 9 in Appendix. The palaeomagnetically relevant minerals are then the iron-oxides, the chromites and the pentlandite for its common association with the ferromagnetic

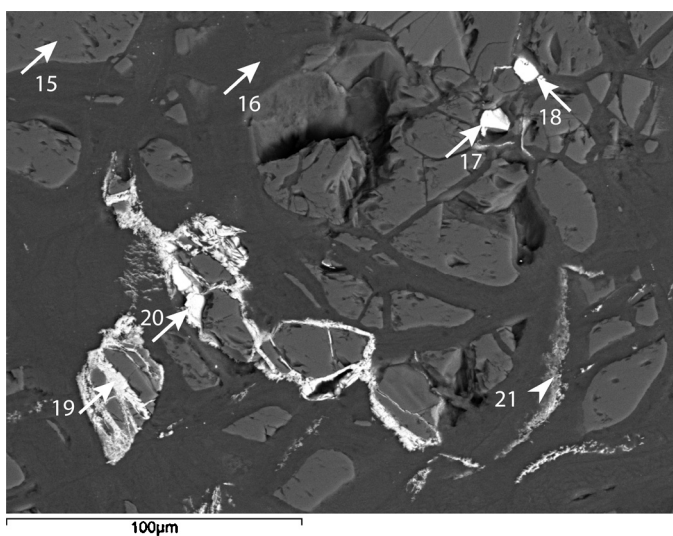


Fig. 2. Representative scanning electron microscope image of sample SA2-3A. Arrows indicate positions used for EDX-analyses (see Tables 8 and 9 in Appendix).

pyrrhotite. The iron–oxide grains investigated were about $10\text{ }\mu\text{m}$ in size. In order to be able to distinguish better between magnetite and pyrrhotite in case of its presence, we have chosen to demagnetize the vast majority of the samples thermally as opposed to AF.

4.2. IRM, backfield and hysteresis

The IRM acquisition curves (Fig. 3) show a representative example) show in most cases a saturation around 200 mT, both in BB and in SA. The back-field curves show a coercivity of remanence H_{cr} of about 34 mT, with very little variation between samples. The saturation magnetization lied between $0.017\text{ A m}^2/\text{kg}$ and $1.0\text{ A m}^2/\text{kg}$, with an average of $0.44\text{ A m}^2/\text{kg}$.

The hysteresis curves have been corrected for their paramagnetic components and then been used to calculate the saturation magnetization M_s , the remanent saturation magnetization M_{rs} , the coercivity H_c and the coercivity of remanence H_{cr} . The ratio M_{rs}/M_s is plotted against H_{cr}/H_c in the Day plot (Day et al., 1977) in Fig. 4, along with theoretical curves for mixtures of SD and MD grains of magnetite with different grain size end members after Dunlop (2002). Dunlop (2002) tested his theoretical curves against

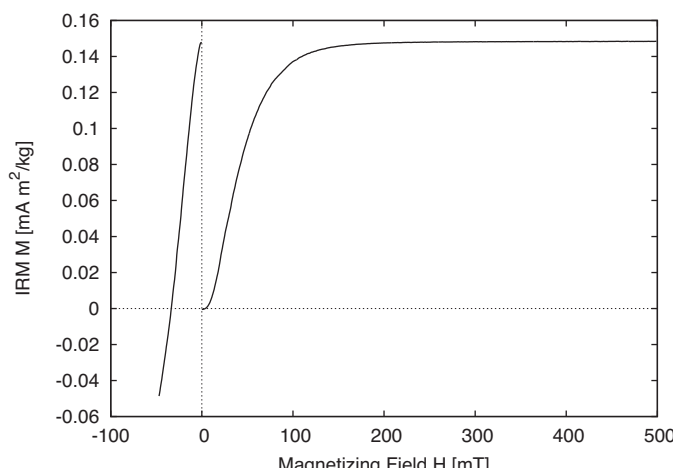


Fig. 3. Representative isothermal remanent magnetization acquisition and back-field curve (sample BB1-6).

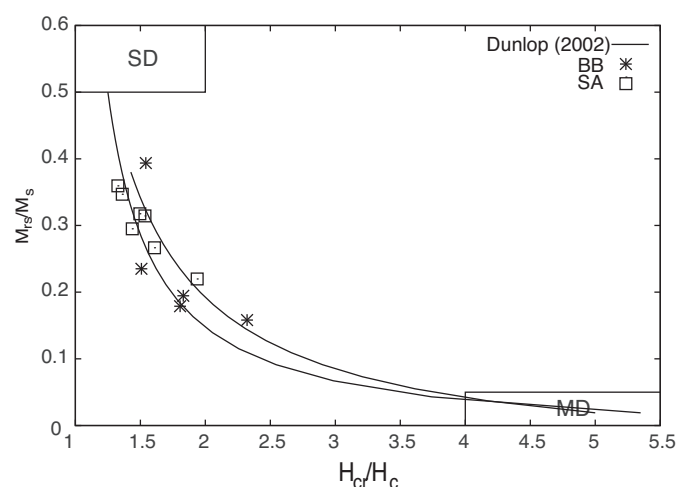


Fig. 4. Day plot of BB and SA samples and theoretical curves for SD + MD mixtures after Dunlop (2002).

data from serpentinized peridotites and found that his peridotites fell on a novel region below the theoretical SD + MD mixing curves. Villasante-Marcos et al. (2003) plotted ‘fresh’ peridotites and a serpentinized peridotite from Ronda on a Day plot and found that the serpentinized sample fell on Dunlop’s (2002b) ‘novel’ region, whereas the ‘fresh’ peridotites followed the SD + MD mixing curve. Similarly, the Beni Bousera and Ceuta peridotites fall very closely on the SD + MD mixing curves for magnetite, with the SA samples generally being closer to the SD region and the BB samples being closer to the MD region. This kind of (grain size dependent) variability of the remanence ratios closely following the theoretical SD + MD mixing curves has also been observed in oceanic serpentinized peridotites (Maffione et al., 2014).

4.3. Thermomagnetic curves

Fig. 5 shows representative thermomagnetic curves. All curves show a Curie temperature T_C of about $580\text{ }^\circ\text{C}$, which is indicative of magnetite. The curves show chemical changes that destroys magnetic minerals (probably magnetite) upon heating, in some of them not appreciably (like BB1-8, Fig. 5(a)), but in others more prominently (like SA8-7, Fig. 5(c)). Fig. 5(b) shows that in sample BB5-9, a small amount of a new magnetic phase is created with a Curie temperature of about $320\text{ }^\circ\text{C}$. Other samples also showed the creation of a very small amount of a new magnetic phase with a less clearly defined Curie temperature. The same kind of destruction of magnetite and the formation of a new magnetic phase with $T_C \approx 350\text{ }^\circ\text{C}$ has been observed by Villasante-Marcos et al. (2003) with the Ronda peridotites.

Fig. 6 shows the results of all the low temperature experiments. In these experiments, the samples have been cooled to 5 K and have then been saturated by applying a magnetic field of 5 T. After switching the external field off, the remanent magnetization of saturation M_{rs} of the sample has been measured whilst heating it up to room temperature. The plot clearly shows the Verwey transition of magnetite around 120 K in all four samples. In addition, two of the samples (one from BB and one from SA) show an increase in slope between 35 K and 50 K.

5. Thermal demagnetization behaviour

The majority of the samples has been demagnetized thermally. The initial NRM ranged from 4.47 mA/m to 15 A/m (median: 260 mA/m). Monitoring the bulk magnetic susceptibility of the

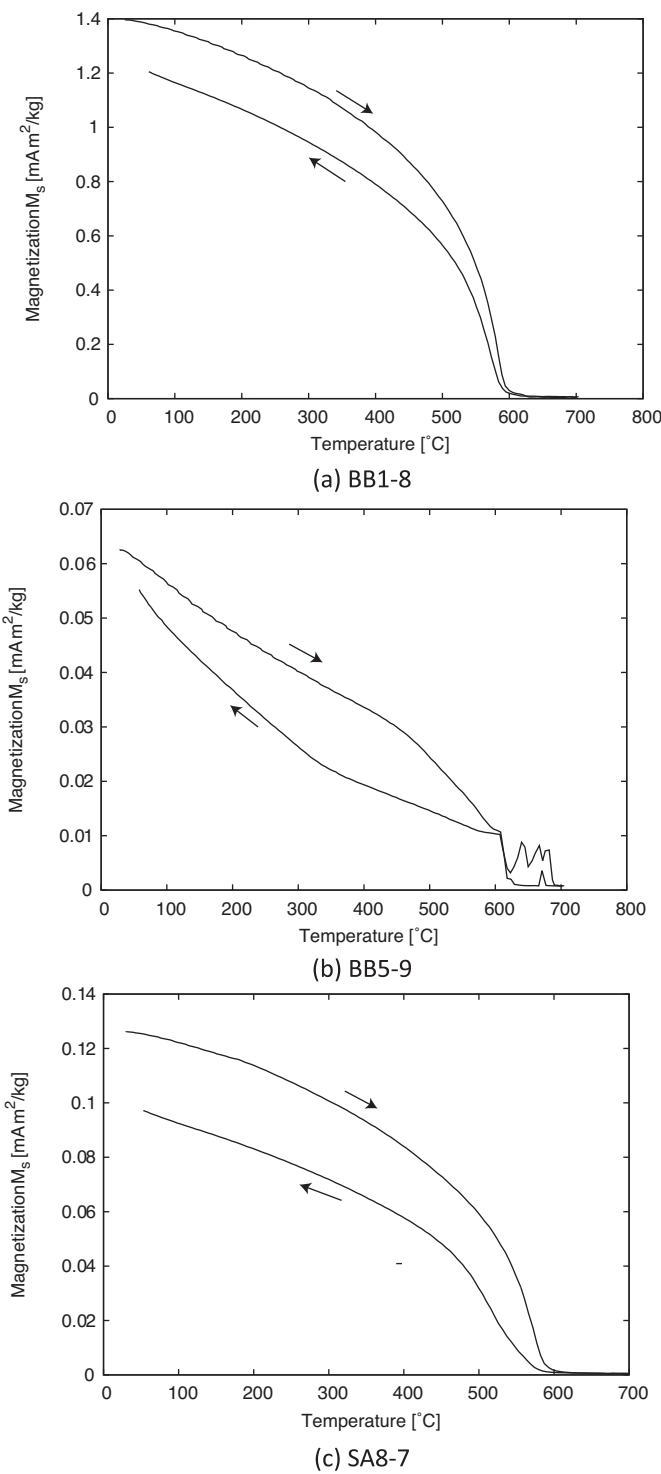


Fig. 5. Representative thermomagnetic curves for heating and cooling.

samples (Fig. 7) showed a very slight increase in susceptibility starting around 200 °C for SA and a moderate increase starting around 300 °C in BB, both reaching a maximum at around 550 °C. This did not have a recognizable effect on the stability of the magnetic components, however.

Most samples showed a very weak component at very low temperatures that was found to contain no useful palaeomagnetic data (see section 5.1). After cleaning this first component, the samples still showed a heterogeneous palaeomagnetic behaviour one or more, often mutually overlapping, magnetic components: Samples

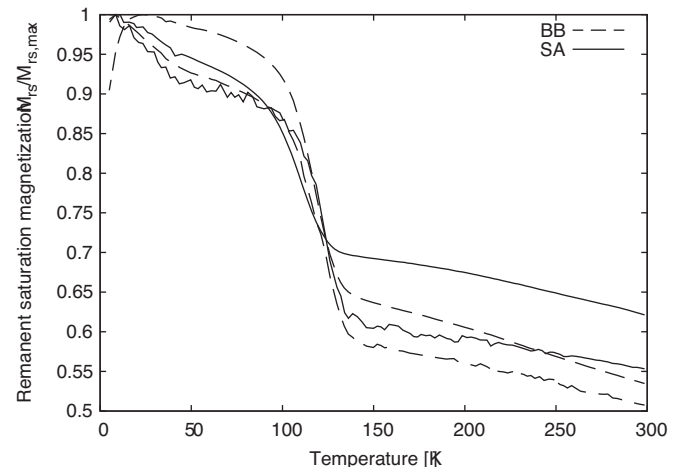
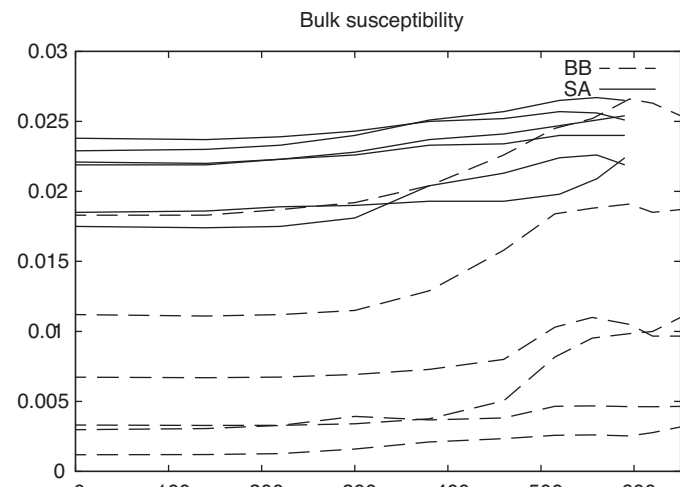
Fig. 6. Remanent saturation magnetization M_{rs} during heating of two BB and two SA samples from 5 K to ambient temperature.

Fig. 7. Mean bulk susceptibility of sites.

from BB had either one or two components and samples from SA had one, two or three components. All of these components have been analyzed and are described in the following.

An overview of the median unblocking temperatures of the three components is shown in Table 2, and the numbers of samples belonging to them are summarized in Tables 3 and 4.

5.1. Very low temperature component

Most samples showed a magnetic component (in some cases more, in others less pronounced) at very low temperatures below 180 °C in BB and, to a lesser degree, below 140 °C in SA (see Fig. 19 in

Table 2

Median temperature ranges used to calculate linear fit lines. LT: low temperature; IT: intermediate temperature; HT: high temperature.

No. of comp.	Site	Comp.	Temperature range
1	BB		180–600 °C
			140–605 °C
2	BB	LT	180–460 °C
		HT	535–600 °C
2–3	SA	LT	140–420 °C
		IT	460–575 °C
		HT	533–603 °C

Table 3

Number of samples from Beni Bousera with the given number of components. Numbers in parentheses is the number of samples that showed directions clustering closely together.

Site	N	1 component	2 components	Rejected
BB1	9	0 (0)	8	1
BB2	9	3 (2)	4	2
BB3	8	2 (1)	6	
BB4	9	2 (0)	6	1
BB5	9	3 (2)	5	1
BB7	9	6 (6)	2	
BB8	8	5 (1)	2	1
Total	60	21 (12)	33	6

Appendix). These directions show a very high dispersion but nevertheless cluster around nearly 90° inclination in BB and around a north-west direction in SA. In the case of BB, there was no correlation between the number of components of the sample and the direction of the very low temperature component. In SA, the mean direction of this component coincides very roughly with the NRM of most samples. The very high dispersion suggest that the measurement of the first few temperature steps may be influenced by a VRM that was acquired in the lab. Therefore, the remanent magnetizations below these temperatures have not been taken into account for any of the calculated directions following below.

5.2. One component (BB and SA)

21 samples of BB (35%) and 21 samples of SA (38%) had only one component. In BB, these samples had unblocking temperatures between 595 °C and 620 °C, and in four cases 680 °C (median: 600 °C, Fig. 8(d)) and in SA they had unblocking temperatures between 560 °C and 640 °C (median was 605 °C). Directions have been calculated using an anchored line-fit for the temperature range 180–595 °C and 140–595 °C, respectively.

As can be seen in Fig. 9, the directions of most of the samples (BB: 12, SA: 14) cluster around a common, roughly north-trending direction (normal polarity). In the case of BB, the mean declination of these 'clustering' samples is virtually 0°, but in the case of SA, it is slightly negative (i.e. slightly 'off' to the west). Some of the samples showed very disperse directions (either polarity), though, and were not included in the calculation of a mean direction.

5.3. Two components (BB)

33 samples of BB (55%) showed two magnetic components, a low temperature (LT) component that is roughly north, and a high temperature (HT) component that is rotated and may be normal or reversed polarity (see Fig. 8(a) and (c)). The LT component showed a linear trend from 180 °C up to a temperature between

Table 4

Number of samples from the Sarchal cliffs with the given number of components. Numbers in parentheses is the number of samples that showed directions clustering closely together. In cases where two components where visible, the higher temperature component could either be identified with the IT or the HT component, and the respective numbers are given in the table.

Site	N	1 component	2 components (IT)	2 components (HT)	3 components	Rej
SA1	7	4 (4)			2	
SA2	9	6 (4)		3		
SA3	8	3 (0)			3	2
SA5	7	2 (2)	1	1	2	1
SA6	8	4 (4)			4	
SA7	8	1 (0)	3	4		
SA8	8	1 (0)	6	1		
Total	55	21 (14)	10	9	11	3

340 °C and 555 °C (median was 460 °C). The HT component then showed a linear trend starting between 380 °C and 575 °C (median: 535 °C) to its unblocking temperature between 555 °C and 620 °C (median: 600 °C, Fig. 8). Sometimes the two components overlapped. Directions of the LT component have been calculated using a non-anchored line-fit using a temperature range from 180 °C to the highest temperature of the linear trend for each sample. Directions of the HT component have all been calculated using an anchored line-fit on the temperature range 535–595 °C wherever possible, and in some cases on 555–595 °C or 575–600 °C.

The LT component is northward (normal polarity) and shows a very low dispersion (Fig. 11(a)). The HT component is either normal polarity and rotated westward by roughly 90°, or reversed polarity and rotated eastward by roughly 90°. The normal polarity HT directions show very little dispersion, whilst the reversed polarity directions show a considerable dispersion. The directions of LT and HT components along with their mean directions (calculated separately for normal and reversed polarity directions) are shown in Fig. 11(a).

5.4. Two to three components (SA)

31 samples of SA (56%) had either two or three components: a low temperature (LT), an intermediate temperature (IT) and a high temperature (HT) component. The number of visible components did not correlate with the degree of serpentinization.

In 11 samples (20%), the presence of all of these three components could clearly be seen in the Zijderveld plots (see Fig. 10(b) and (c)) and linear fit lines could be calculated. In some cases, however, the presence of three components could only be deduced by a curvature of the Zijderveld plot (Fig. 10(a) and (d)): In Fig. 10(a) a LT and a HT component are linear but in-between one finds an "S"-shaped part. Such a shape is best explained by three components with the unblocking temperature spectrum of the intermediate component completely overlapping with those of the other two components (see e.g. Kirschvink, 1980 for similar considerations). Similarly, Fig. 10(d) shows linear LT and IT components but the highest few temperature steps describe a curve which is best explained by another HT component that completely overlaps with the IT component. In these cases, linear fit lines could not be used to calculate both the HT and IT component, but best-fit great circles have been used instead to obtain an estimate of the HT component, whenever possible (Halls, 1976).

In yet other samples, only two components were visible (Fig. 10(a) and (d)), in which case the first component was always the LT component and the second component could be identified as either the IT or the HT component according to its direction.

The LT component showed a linear trend (see Fig. 8) on the temperature range from 140 °C to 340–490 °C (median: 420 °C). The IT component showed a linear trend starting at 380–560 °C (median: 460°) and ending at 520–605 °C (median: 575 °C). The HT component showed a linear trend starting at 380–575 °C (median: 533°) and ending at 575–625 °C (median: 603 °C). Sometimes this led to the necessity of using just a single point to define a fit line to the origin. The temperature ranges used for the calculation of the directions have been chosen for each sample individually. The LT component, however, was always calculated starting at 140 °C. For the LT and IT components non-anchored and for the HT component anchored line-fits were used.

The LT component nearly always lies between north and north-west and shows relatively little dispersion ($\alpha_{95} = 5.1^\circ$, Fig. 11(c)). The HT component shows equally little dispersion ($\alpha_{95} = 9.6^\circ$) and is approximately northward. Looking at the LT and the HT components together, a striking feature is that the dispersion they show, roughly describes a great circle from a point in the north with a low inclination to a point in the west with a higher inclination. The IT

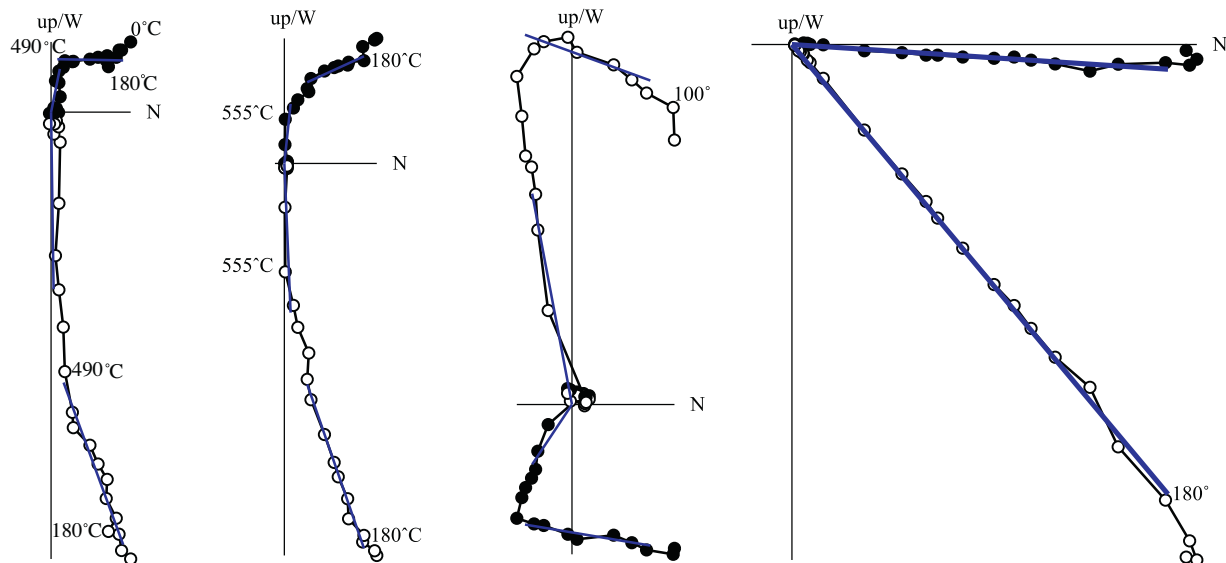


Fig. 8. Zijderveld plots of BB. Solid lines are best fit lines.

component directions all lie in the southern hemisphere, and most lie south-west. All but five are reversed polarity. They show a large dispersion ($\alpha_{95} = 19.8^\circ$), which is due to the fact that in most samples the IT overlapped with the LT and/or the HT component. Hence, IT directions should be considered only very rough estimates.

5.5. Rejected samples

Six samples from BB (10%) and three samples from SA (5%) have not been taken into account for the palaeomagnetic analysis, because they showed uncoherent palaeomagnetic components that were very different to the rest of the samples.

6. Alternating field demagnetization

A number of specimens have been AF demagnetized. This permitted to compare the directions of the magnetic components between the two demagnetization methods. This way, the unblocking temperatures could be related to the coercivities of the respective mineral, which greatly helps the mineralogical interpretation of the remanences (see Section 7.1).

In general, thermal and AF demagnetization gave similar results, but because of technical problems with the SQUID, high field data (>30 mT) had to be discarded and therefore directions obtained by AF have not been taken into account for final calculation of the mean directions. For most of the AF demagnetized specimens, a second specimen of the same sample has been thermally demagnetized as well. Fig. 11(b) and (d) shows the directions as obtained by AF with those obtained by thermal demagnetization.

6.1. Beni Bousera

In BB, all samples demagnetized by AF showed two stable components (Fig. 11(b)), a low coercivity (LC) component that unblocked at around 9–12 mT and a high coercivity (HC) component that unblocked at applied fields above 30 mT (the exact coercivity could not be determined due to technical problems). Generally, the LC component had a northward direction very similar to the LT component of thermally demagnetized samples with two components.

The high coercivity component either had a west normal-polarity or an east reversed-polarity direction, and hence

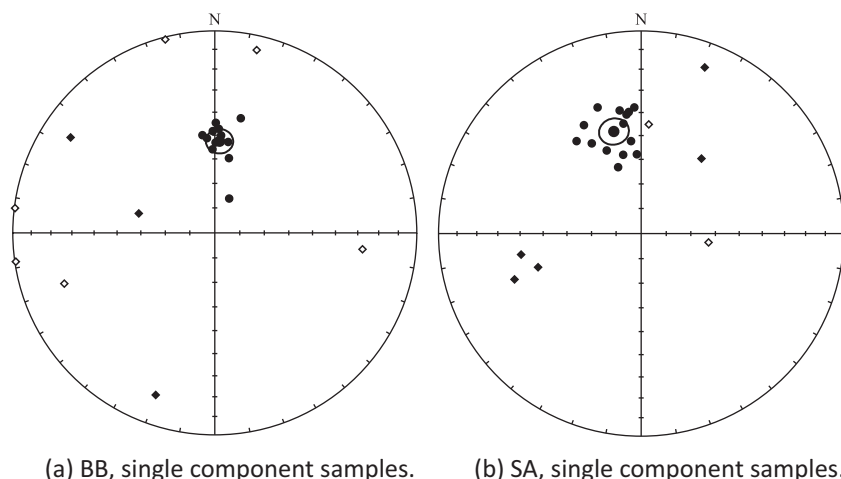


Fig. 9. Directions (without tectonic correction) of samples that had only one component. Circles are roughly north trending directions, diamonds are non-north trending directions. Mean direction of the roughly north-trending directions are indicated along with the α_{95} confidence level. Filled symbols: normal polarity, unfilled: reversed polarity.

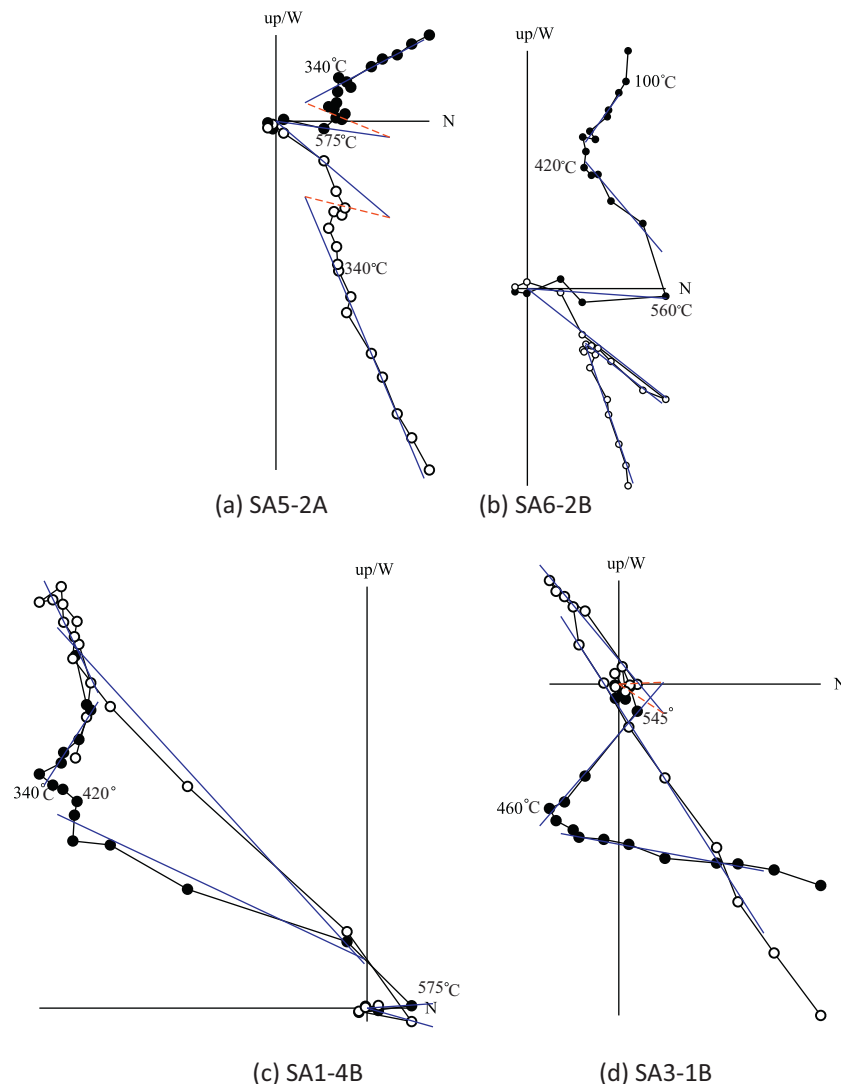


Fig. 10. Zijderveld plots of SA samples where three components (LT, IT, HT) are visible. Solid lines are best fit lines. The dashed lines are hypothetical components that might cause the observed curvature due to overlap with the other components.

corresponds to the HT component of the thermally demagnetized samples. Deviating from this rule, however, there were two samples where the LC and HC components were 'swapped', in the sense that the LC component was westward rotated and the HC component was north, as shown in Fig. 12. Moreover, two samples that showed two clearly distinguishable component in AF, showed only one component in thermal demagnetization.

6.2. Ceuta

In SA, all samples showed either two or three stable components (Fig. 11(d)). A low coercivity component that unblocked at 9–12 mT was present in all samples and had north to westward directions with normal polarity. This component can be identified with the LT component of the thermally demagnetized samples. In cases where they were three components, an intermediate coercivity (IC) component tended to be south, reversed-polarity and a high coercivity (HC) component tended to be roughly north with a normal-polarity and low inclination. In samples that showed only two components, the higher coercivity component showed the same behaviour as either the IC or the HC component. Hence, in general, the IC component of AF demagnetized specimens can be identified with the IT component of thermally demagnetized specimens and the HC

component can be identified with the HT component. In one sample was this behaviour 'swapped' again, and seven samples that showed only one component in thermal demagnetization showed two or even three distinguishable components in AF.

6.3. Relation between unblocking temperature and coercivity

Fig. 13 shows the normalized intensity of the sum of the partial TRM's (pTRM) during the thermal demagnetization. Most samples were completely demagnetized at around 595 °C, but three samples (all of BB) had an unblocking temperature of about 680 °C (note that as the plot shows the sum of pTRMs, experimental noise at high temperatures incorrectly shows up as apparent high intensities at high temperatures – as this is just an artefact, the unblocking temperatures of the highest temperature component have been determined by the absolute intensities as opposed to the pTRM sums). The plots show that there are at least two populations of unblocking temperatures, one that causes a major decay between 140 °C and 340 °C and another one with a major intensity decay at high temperatures between 535 °C and 595 °C. Depending on the relative prominence of these two populations, samples lose most of their remanence either at low temperatures, or at high temperatures, or showed a quasi-linear decay from 140 °C to 595 °C.

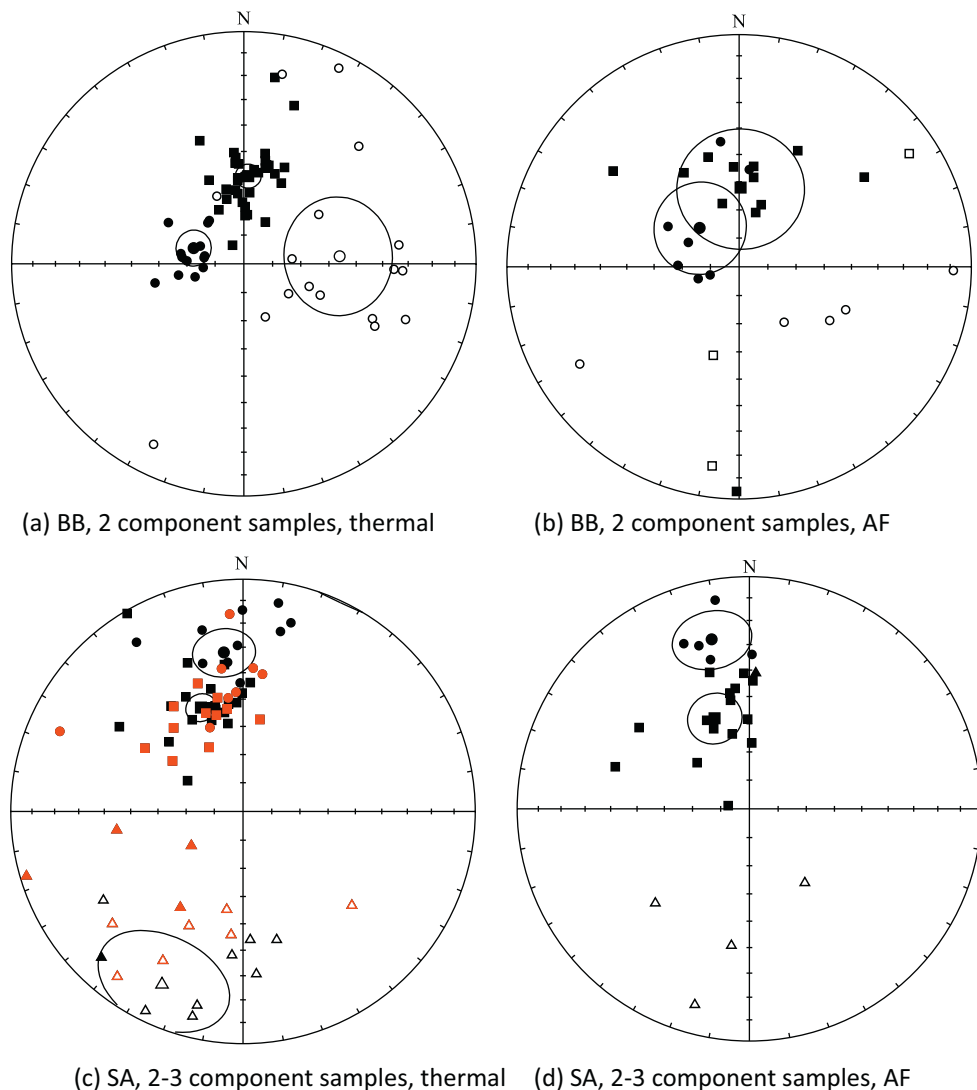


Fig. 11. Directions (without tectonic correction) of samples with 2 or 3 components as obtained by thermal and AF demagnetization, respectively. Circles represent HT component, squares LT component and triangles are IT component. Mean directions are indicated along with the α_{95} confidence level and have been calculated separately for normal (black symbols) and reversed polarity (open symbols). Red symbols indicate SA samples where all three components (LT, IT, HT) were clearly visible (the others are samples where only two components were clearly visible). Filled symbols: normal polarity, unfilled: reversed polarity. (For interpretation of the references to color in this figure legend, the reader is referred to the web version of this article.)

Plots of the remanence intensity decays during AF demagnetization of samples demagnetized with the SQUID are shown in Fig. 13(c) and (d) (measurements above 30 mT have been removed). Again, two coercivity populations can be distinguished, one with a major decay between 0 and 9 mT (this is somewhat less pronounced for the SA samples) and another one causing a slow decay between 12 and 30 mT or more, where again, the relative importance of the two populations varied from sample to sample.

Comparing the specimens of samples that had both AF and thermally demagnetized, a clear correlation between the two unblocking temperature and coercivity populations could be seen: The intensity decay at low temperatures corresponded to the intensity decay of low coercivities and the one of high temperatures corresponded to high coercivities.

To make the correspondence between coercivity and blocking temperature, sample BB7-6A, has first been partially demagnetized by thermal demagnetization up to 340 °C and then completely demagnetized by AF demagnetization (Figs. 14 and 15). After partial thermal demagnetization, the strong decay between 0 and about 5 mT is not visible anymore.

7. Discussion

7.1. Responsible mineralogy for the NRM

In the SEM/EDX analysis, iron-oxides, chromite and pyrrhotite have been identified as possible candidates for the NRM.

Saddiqi et al. (1995), in their study of the BB peridotites, consider magnetite, titanomagnetite and hematite the most likely magnetic remanence carriers. In this study, however, most samples had an unblocking temperature of around 580 °C and only three samples showed an unblocking temperature of 680 °C. Although, the accuracy of the unblocking temperature determination is relatively low (compare Section 4.3), they clearly favour an interpretation as magnetite as opposed to hematite. Equally, only minute amounts of titanium have been found in the EDX analysis, therefore we do not consider titanomagnetite a likely candidate either.

The unblocking temperature spectra showed in many samples a strong decay below 300 °C (Fig. 13(a)), suggesting the presence of pyrrhotite. However, in the demagnetization, no components compatible with the Curie temperature of pyrrhotite (320 °C, Dunlop

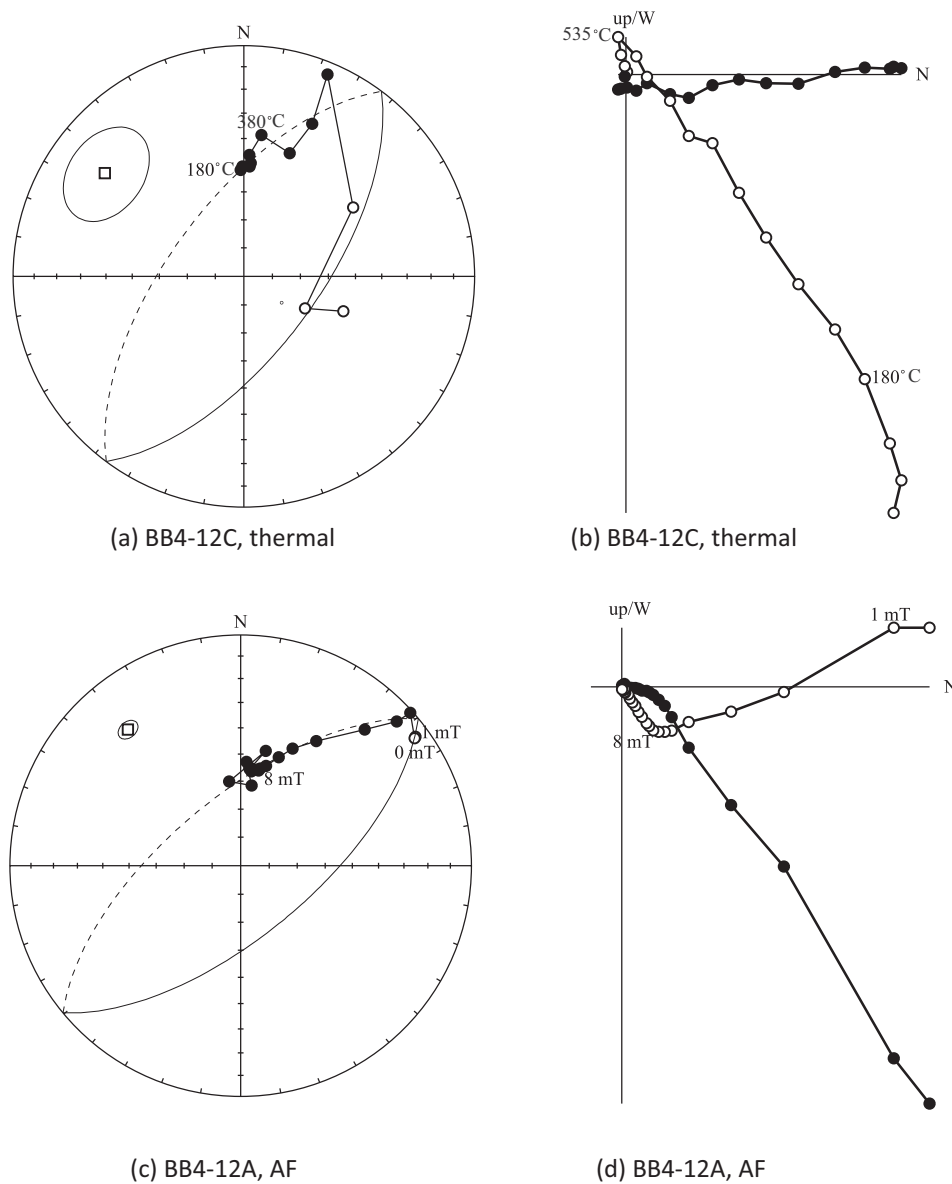


Fig. 12. Paleomagnetic results of two specimens of BB4-12, demagnetized thermally and by AF, respectively.

and Özdemir, 2009) could be observed: All the LT components persisted well above 400 °C and often showed overlap with the IT/HT component at even higher temperatures. Therefore, if pyrrhotite carries a significant portion of the NRM, it has recorded the same magnetic signal as one of the other magnetic minerals.

The iron-poor endmember of the chromite series ($\text{Fe}(\text{Cr}, \text{Fe})_2\text{O}_4$) has a Curie temperature of -185°C that increases with decreasing Cr content (Dunlop and Özdemir, 2009) until it reaches $T_C = 580^\circ\text{C}$ for the iron-rich endmember (magnetite). Therefore, Cr may play a similar role as Ti, in reducing the unblocking temperature of magnetite, although we do not believe that this is the dominant mechanism for producing the different unblocking temperatures for the reasons described below.

The unblocking temperatures of most samples and the IRM experiments suggest magnetite as the principal carrier of the NRM. Notably, there is a significant amount of multi-domain (MD) grains of magnetite, as can be seen by the very low coercivities in Fig. 13(c) and (d) and the Day plot Fig. 4.

We believe that the there are two major grain size populations of magnetite that are responsible for the observed magnetic

components in the vast majority of the samples. One of them is in the MD range and is responsible for the LT component, the other one is in the SD or PSD range and is responsible for the HT and IT components. This hypothesis is supported by the following observations:

1. In the Day plot (Fig. 4), the samples fall almost perfectly on the theoretical magnetite SD + MD mixing curves of Dunlop (2002). Although Dunlop (2002) found that some serpentized peridotites fell on a novel region below the theoretical curve (for which he does not have an explanation), we believe that in our case the magnetic properties of the peridotites are dominated by SD and MD magnetite grains so that they follow the theoretical curve.
2. The low temperature experiments (Fig. 6), although they do not reject small contributions of titanomagnetite, give clear indications of pure magnetite through a clearly visible Verwey transition. It is neither shifted from 120 K nor depressed, hence not indicating any Ti content or surface oxidation (Dunlop and Özdemir, 2009). Moreover, the experiments are not indicative of

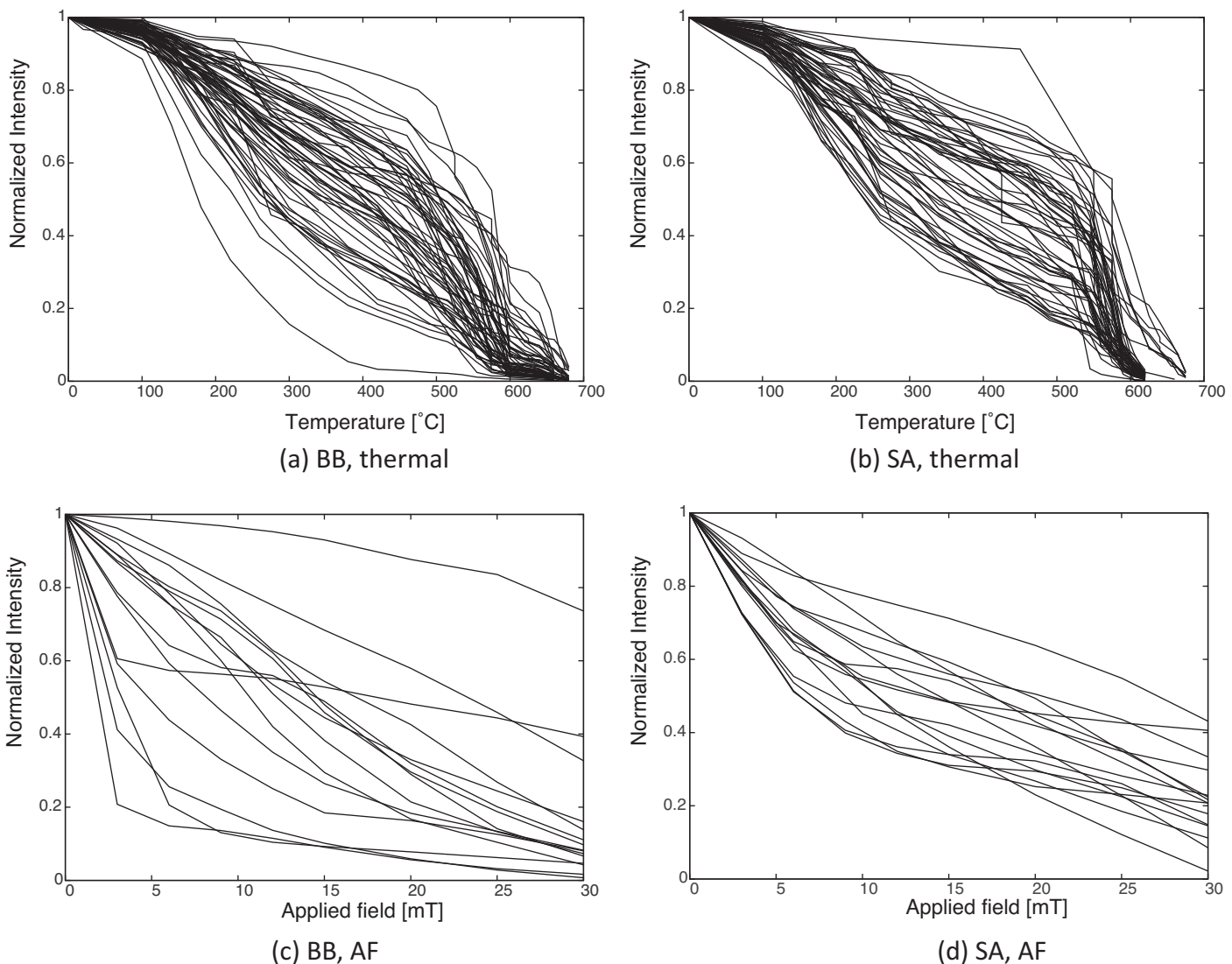


Fig. 13. Normalized intensity of the sum of partial remanent magnetizations during thermal (a, b) and AF (c, d) demagnetization (only SQUID).

pyrrhotite, which has a transition from a monoclinic to trigonal crystal structure around 35 K (Rochette et al., 1990). There is a change of slope around that temperature, however, the transition of pyrrhotite causes a very sharp increase in M_{rs} over a very narrow temperature range (over about 5 K), which is not seen in Fig. 6. It should be noted that (Dunlop and Özdemir (1997, and references therein) show very similar low temperature thermoremanent curves for annealed crushed magnetite that exhibit just this change of slope around 50 K.

3. The very low coercivities of the LC component are likely due to MD grains. The correspondence in direction of the LC component in AF demagnetization and the LT component in thermal demagnetization and the correlation between the intensity decay at low coercivities and at low temperatures support an identification of these MD grains with the LT component.
4. Similarly, both the IT and the HT components in SA have high unblocking temperatures and high coercivities that point to grains in the PSD/SD range. Both components had very similar unblocking temperatures and coercivities. These similarities in their magnetic properties point to similar chemical compositions and similar grain sizes/shapes.
5. Fig. 15 suggests that the grains with unblocking temperatures below 340° correspond to very low coercivities (in this

particular sample about 5 mT), and hence probably to MD grains. The AF intensity decay curve after partial thermal demagnetization in Fig. 14 has the shape typical of a PSD or SD grain size distribution. Hence the HT and IT components are probably due to these SD/PSD grains.

We conclude that the different unblocking temperatures of the different components are likely due to different grain size distributions, although Cr or Ti impurities may possibly play a role as well.

7.2. Acquisition of the remanence

According to Villasante-Marcos et al. (2003) and references therein, there were two post-metamorphic serpentinization phases (at least in Ronda), the first formed sub-microscopic magnetite and the second up to millimetre-sized magnetite grains, mainly along fractures. Hence, supposing that first serpentinization phase created SD/PSD magnetite grains, they likely acquired a CRM at the time of their formation ~20 Ma ago. The larger grains from the posterior serpentinization phase are likely in the MD range and should as well carry a CRM from the time of their formation.

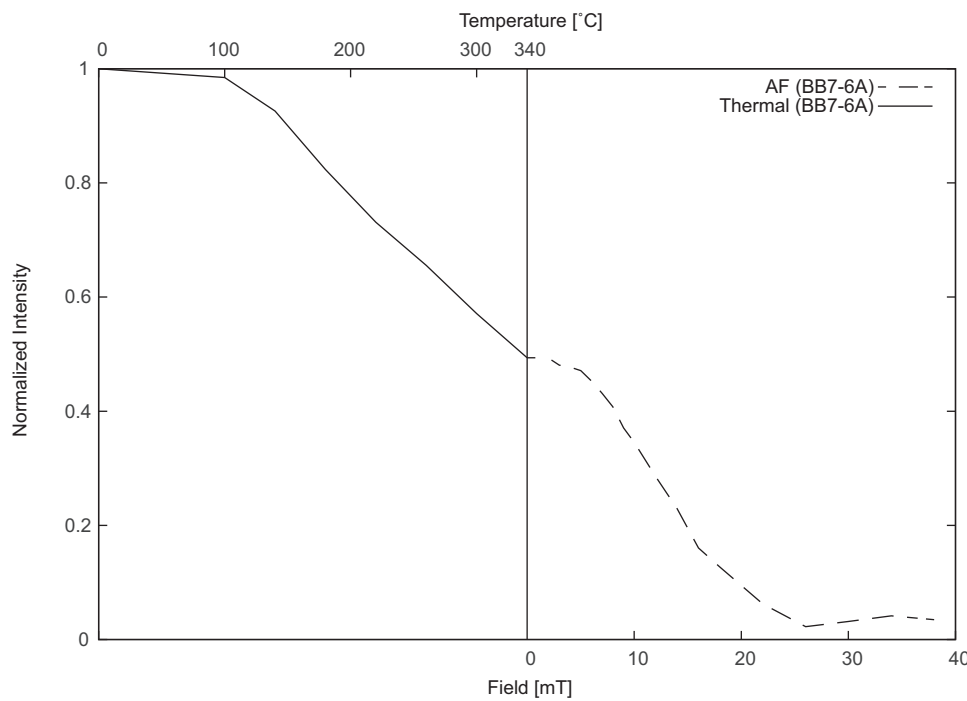


Fig. 14. Normalized intensity of the remanent magnetization of BB7-6A that has first been partially thermally demagnetized and then further demagnetized by AF.

This interpretation as CRMs is contrary to Saddiqi et al. (1995, Beni Bousera) and Feinberg et al. (1996, Ronda), but in line with Villasante-Marcos et al. (2003, Ronda). Saddiqi et al. (1995) and Feinberg et al. (1996) interpret the two magnetic components they found in the Beni Bousera and Ronda peridotites as pure TRMs. Their interpretation implies that the rotations they observed were completely finished by the time the peridotites had cooled to about 450 °C (Saddiqi et al., 1995, Beni Bousera) and 250 °C (Feinberg et al., 1996, Ronda), respectively.

There are, however, various observations that favour our interpretation of CRM's due to two serpentinization phases. The main reason is that some samples showed a very sharply separated components but others show a continuous curvature from LT to HT component. If the acquisition mechanism was a TRM by cooling,

then one would expect a more homogeneous behaviour: on the one hand, if the rotation was slow compared to the cooling time, one should see a curvature in the Zijderveld diagrammes as progressively higher temperatures should have recorded sequential stages of the rotation. On the other hand, if the rotation was fast compared to the cooling time, such a curvature should become very small (i.e. over a very narrow range of blocking temperatures) or completely disappear. Our data, however, shows both of these behaviours (compare Fig. 8(a) and (b)). According to the figures in Feinberg et al. (1996), they apparently observed a heterogeneous behaviour in Ronda, too. By assuming CRM to be the acquisition mechanism, this behaviour is easily explained: The two serpentinization phases (pre- and post-rotation), formed two different grain-size populations, one of them recording the pre-rotational

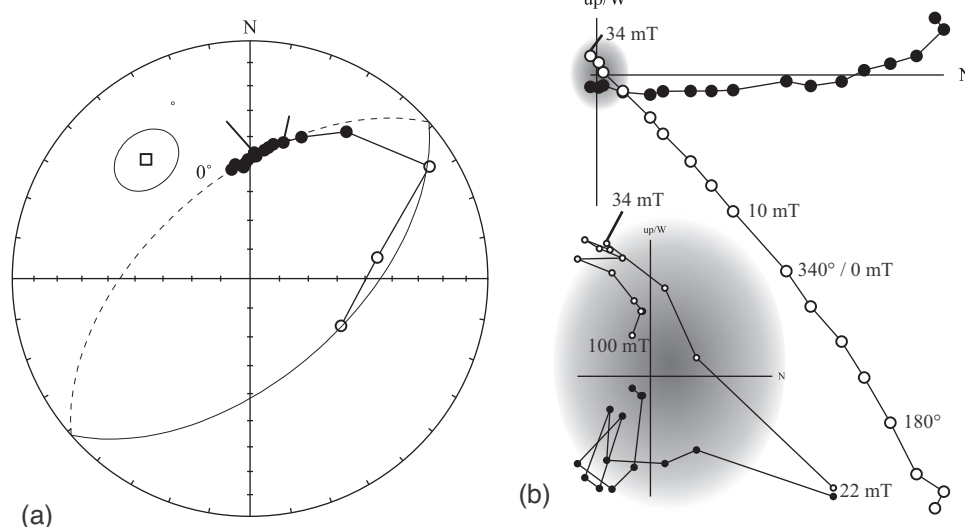


Fig. 15. Paleomagnetic results of sample BB7-6A, demagnetized first partially thermally and then by AF. The Zijderveld plot goes to the origin at higher fields, but points have not been plotted for better visibility.

and the other one recording the post-rotational direction. Depending on the overlap of these two grain-size spectra (or equivalently blocking temperature spectra) one will have either overlapping directions or sharply separated directions.

In the case of the LT and HT components, the two serpentinization phases formed very different grain-size populations (one mainly in the MD range and one mainly in the PSD/SD range), that in many cases did not show much overlap – hence the components very easily isolated. On the other hand, in the case of the IT and HT components that both formed during the posterior serpentinization, both IT and HT components formed very similar grain-size spectra, but the HT component is slightly biased towards larger grains (i.e. with higher blocking temperatures). Hence, they are strongly overlapping and not easily isolated.

7.3. Palaeomagnetic directions

Due to the existence of previous negative fold tests of other authors in the Beni Bousera (and also Ronda) peridotites (Saddiqi et al., 1995; Feinberg et al., 1996; Villasante-Marcos et al., 2003), we consider only “in situ” directions. As shown in those works, all the remanences are younger than the foliation/anticline formation. The negative fold test in the BB peridotites (Saddiqi et al., 1995), was performed using 6 sites showing a reversed, rotated component, where α_{95} increased from 10.3° to 22.3° (and k decreased from 43 to 10) after tectonic correction. As a rough quality control, this has been checked for the current study using only 4 sites from BB and SA using local foliation measurements. The angular dispersion of mean directions (Table 5) increased in both SA and BB after applying the tectonic correction: from 7.3 to 7.7° (SA) and from 25.1 to 63.7° (BB).

7.3.1. Beni Bousera (BB)

In the case of Beni Bousera, the samples with only one component showed either a non-rotated direction or a completely dispersed direction. The dispersed directions have not been considered useful for palaeomagnetic purposes. They could be isothermal remanent magnetizations (IRM) that hence have not preserved their original magnetizations. The clustering directions have probably only preserved a recent (post-rotation) remanent magnetization.

In the same way, the LT component of those samples with two components is probably a recent magnetization. LT components of these samples and the NRM of those samples with only one component can be considered to have been recorded by the same (re-)magnetization event. Both have been used to calculate site mean directions using Fisher's statistics (Fisher, 1953). The mean direction of them is $D = 2.4^\circ$, $I = 56.7^\circ$ and $\alpha_{95} = 5.4^\circ$, which confirms that there is no vertical axis rotation nor tilting, as the expected declination is 0° for the last 20 Ma and the observed inclination coincides with the expected one for the last few Ma (see Section 7.4). All (uncorrected) site mean directions are summarized in Table 5 plotted in Fig. 16.

The HT component of samples with two components is likely a pre-rotation remanent magnetization. Site mean directions have been calculated for these samples using the magnetization vectors as obtained by anchored line fits wherever possible. In some cases the HT component was either too small or overlapped with the LT component, however. In these cases (see Fig. 17), converging remagnetization circles have been used to obtain an estimate of the HT component using the method of Kirschvink (1980) that combines best-fit lines with best-fit planes.

Generally, HT components of a single site had the same polarity. The respective mean directions of normal and reversed polarity sites are given in Table 6 along with all the other mean directions of the different components. Notably, normal polarity sites have been

Table 5
Summary of site mean directions (without tectonic correction).

Site	Comp.	Nu/N	D	I	α_{95}	k
BB1	LT	8/9	358.2	65.4	6.1	83.9
BB2	LT	6/9	355.9	65.4	11.3	35.9
BB3	LT	7/8	11.4	56.4	11.4	29.0
BB4	LT	6/9	3.9	56.5	7.0	93.6
BB5	LT	7/9	7.5	50.6	12.6	23.8
BB7	LT	8/8	1.6	51.6	5.7	96.3
BB8	LT	3/8	355.7	50.4	18.6	45.1
BB1	HT	8/9	289.8	72.5	4.7	137.2
BB2	HT	4/9	269.4	65.3	13.0	51.2
BB3	HT	5/8	90.2	-62.3	15.3	26.1
BB4	HT	4/9	146.4	-49.7	54.5	3.8
BB5	HT	5/9	92.6	-64.7	22.6	12.4
BB7	HT	2/8	102.4	-36.3		
BB8	HT	3/8	128.9	-48.5	22.3	31.7
SA1	LT	7/7	335.1	49.9	9.1	44.8
SA2	LT	7/9	333.1	44.1	12.7	23.6
SA3	LT	3/8	342.3	51.5	26.7	22.4
SA5	LT	6/7	343.4	42.0	19.5	12.8
SA6	LT	8/8	339.5	56.0	7.2	59.8
SA7	LT	7/8	339.5	49.0	12.2	25.3
SA8	LT	7/8	348.8	51.2	4.6	174.5
SA1	IT	1/7	205.2	-44.7		
SA3	IT	3/8	166.3	-49.5	38.5	11.3
SA6	IT	2/8	223.0	-19.3		
SA7	IT	3/8	175.7	-41.7	12.0	106.6
SA8	IT	5/8	200.8	-19.1	23.3	11.7
SA1	HT	2/7	356.3	31.6		
SA2	HT	3/9	352.3	38.1	11.7	112.7
SA3	HT	3/8	352.8	35.0	4.1	902.0
SA5	HT	3/7	2.5	31.7	13.1	90.1
SA6	HT	4/8	352.8	46.1	13.7	45.8
SA7	HT	4/8	8.8	15.9	9.0	105.4
SA8	HT	1/8	347.3	21.0		

found for the first time and were roughly antipodal (i.e. westward) to the reversed polarity directions.

7.3.2. Ceuta (SA)

From the considerations outlined in Section 5, and from analogy with BB, the palaeomagnetic directions of one-component samples of SA (in particular the clustering ones) are likely a recent (due to the posterior serpentinization phase) remanent magnetization, as is the LT component of SA group 3 samples. Similarly as in BB, we assume that directions of single component samples of SA and the LT component of samples with multiple components have recorded the same event. The six samples of that showed very disperse single components are again considered IRMs and are not been taken into account for the calculations of mean directions. The mean direction of LT components directions is $D = 340.2^\circ$, $I = 49.2^\circ$ with $\alpha_{95} = 4.4^\circ$.

The IT component of SA showed in many cases a significant overlap with one or both of the other components, such that no reliable direction could be obtained. Nevertheless, 15 samples had a clear,

Table 6

Mean directions (without tectonic correction) of the different isolated components. Comp.: component (LT: low temperature; IT: intermediate temperature; HT: high temperature); N: number of samples; D: declination; I: inclination; BB: Beni Bousera; SA: Sarchal cliffs.

Site	Comp.	N	D	I	α_{95}	k
BB	LT	7	2.4	56.7	5.4	124.6
BB	HT normal	2	278.0	69.2		
BB	HT reversed	5	114.2	-54.3	17.8	19.5
BB	HT antipodes	7	291.0	58.0	13.1	22.0
SA	LT	7	340.2	49.2	4.4	191.5
SA	IT	5	196.6	-36.6	22.9	12.1
SA	HT	7	356.4	31.6	9.1	45.4

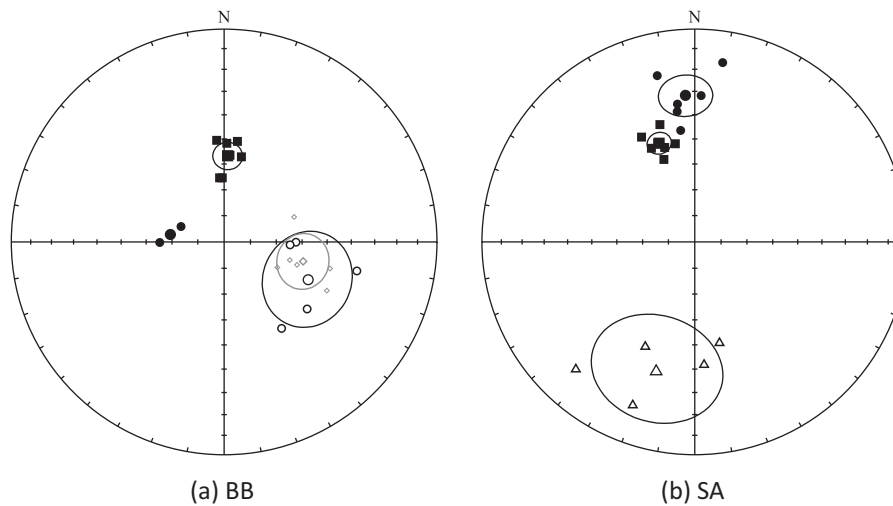


Fig. 16. Site mean directions (without tectonic correction) of BB (a) and SA (b) sites. Squares: group 1a and LT components of group 2 (BB) and 3 (SA); circles: HT components of group 2 (BB) and 3 (SA); triangles: IT component of group 3 (SA); grey diamonds: high temperature component from [Saddiqi et al. \(1995\)](#). Open symbols indicate reversed polarity, mean directions are indicated along with α_{95} confidence levels.

non-overlapping IT component. These have been used to obtain estimates of site mean directions. The mean direction of all sites is then $D = 196.6^\circ$, $I = -36.6^\circ$ and $\alpha_{95} = 22.9^\circ$.

In four cases, the HT component showed considerable overlap and a low signal-to-noise ratio. Therefore, converging remagnetization circles had to be used to obtain estimates of the HT components of these samples (see Fig. 17). The mean direction of the HT component of all sites is $D = 356.4^\circ$, $I = 31.6^\circ$ and $\alpha_{95} = 9.1^\circ$.

All calculated (uncorrected) mean directions for each of the components are given in Table 6.

7.3.3. Palaeosecular variation averaging

Despite the limited number of sites involved, the mean directions listed in Table 6 can be regarded to sufficiently average the paleosecular variation (PSV) of the geomagnetic field, because of the positive reversal tests of the IT and HT components, the α_{95} -envelope reliability criteria proposed by [Deenen et al. \(2011\)](#) and the effect that a CRM acquisition mechanism leads to a smoothing of the PSV signal at the specimen scale. Overlapping components and CRM acquisition are not ideal conditions for analysis of the

geomagnetic dispersion or other PSV estimates, but for tectonic purposes, our results are useful.

7.4. Rotations and tilt

The expected directions for the north-west African craton for 20 Ma is, according to [Torsvik et al. \(2012\)](#), $D = 359.9 \pm 3.0^\circ$, $I = 48.5 \pm 3.0^\circ$ for BB and $D = 359.9 \pm 3.0^\circ$, $I = 49.2 \pm 3.0^\circ$ for SA. For the last 5 Ma the expected direction is $D = 0.0 \pm 2.3^\circ$, $I = 53.3 \pm 2.0^\circ$ for BB and $D = 0.0 \pm 2.3^\circ$, $I = 53.9 \pm 1.9^\circ$ for SA. Hence, the declination can be considered 0° within its experimental error for the last 20 Ma. Although, the evolution of the palaeodirection is strongly smoothed (with running averages of 20 Ma windows), a trend from slightly lower to slightly higher inclinations is evident that is due to the northward shift of the African plate.

7.4.1. Beni Bousera (BB)

The direction obtained for the HT component of BB, after taking antipodes of the reversed polarity directions, is $D = 291.0 \pm 25.3^\circ$, $I = 58.0 \pm 13.1^\circ$ (see Table 6). Similarly, [Saddiqi et al. \(1995\)](#)

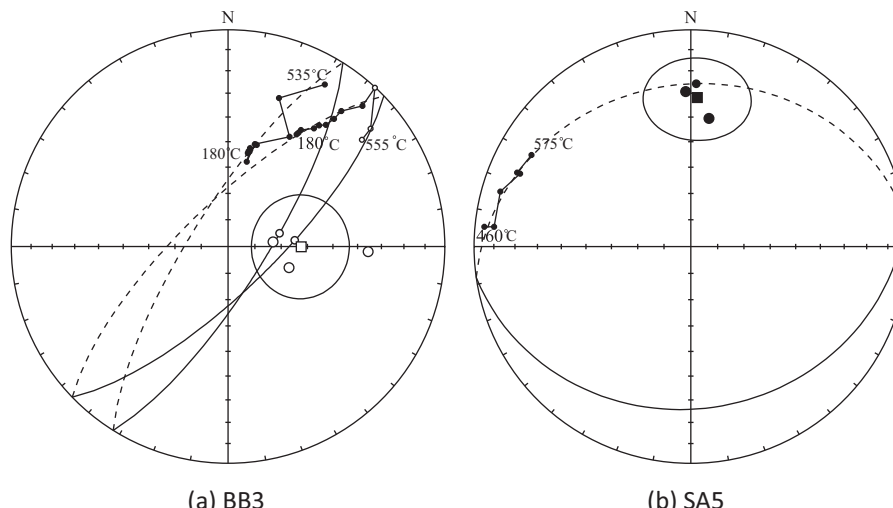


Fig. 17. Calculation of directions of the HT component that overlapped with LT (BB group 2) or IT (SA group 3), respectively, using converging remagnetization circles. α_{95} circles are indicated.

Table 7

Rotations R (observed minus expected declinations; positive values are clockwise rotations) and flattening of inclination F (expected minus observed inclination) parameters with their confidence limits (Demarest, 1983).

Site	Component	Data from	$R \pm \Delta R$	$F \pm \Delta F$
BB	HT	This work	$68.9 \pm 20.4^\circ$	$-9.5 \pm 10.8^\circ$
	HT	Saddiqi et al. ^a	$76.1 \pm 16.2^\circ$	$-10.1 \pm 8.6^\circ$
	HT	Combined	$72.3 \pm 12.1^\circ$	$-10.1 \pm 6.5^\circ$
	LT	This work	$2.4 \pm 8.1^\circ$	$-3.4 \pm 4.6^\circ$
	LT	Saddiqi et al. ^a	$1.3 \pm 8.3^\circ$	$-4.1 \pm 4.6^\circ$
SA	HT	This work	$3.5 \pm 8.9^\circ$	$17.6 \pm 7.7^\circ$
	IT	This work	$-16.7 \pm 23.3^\circ$	$12.6 \pm 18.5^\circ$
	LT	This work	$19.7 \pm 5.9^\circ$	$0.0 \pm 4.2^\circ$

^a The rotations of Saddiqi et al. (1995) have been re-calculated using the expected directions from Torsvik et al. (2012).

obtained a direction of their HT component (after taking antipodes) of $D=283.8 \pm 20.1^\circ$, $I=-58.6 \pm 10.3^\circ$. Using the values given by Torsvik et al. (2012), the HT component gives an anti-clockwise rotation about a vertical axis of $68.9 \pm 20.4^\circ$ and a flattening parameter of $F=-9.5 \pm 10.8^\circ$ (see Table 7), which means that a slight tilt ($<10^\circ$ and posterior to the anticline formation, which predate the remanences) can neither be rejected nor confirmed.

Combining the data of Saddiqi et al. (1995) and of this study, the certainty of the rotation can be improved (see Fig. 16(a)). By taking the antipodes of reversed polarity directions one obtains a mean direction with $D=287.6^\circ$, $I=58.8$, $\alpha_{95}=7.6$, $k=30.4$, which implies an anti-clockwise rotation of $72.3 \pm 12.1^\circ$.

The LT component of BB has a similar inclination of 56.7° (Saddiqi et al. (1995) obtained $I=57.4^\circ$) and a declination of 2.4° . For the expected direction for the last 5 Ma, this represents a flattening parameter of $F=-3.4 \pm 4.6^\circ$, and we can assume no tilt and no rotation for the LT component.

7.4.2. Ceuta (SA)

Both the IT (after taking antipodes) and the HT component of SA have similar, low inclinations ($I=36.6 \pm 22.9^\circ$ and $I=31.6 \pm 9.1^\circ$, respectively).

Using the “in situ” IT/HT mean results from SA listed in Table 6, a reversal test and their quality classification has been performed following McFadden and McElhinny (1990), giving a positive “type C” result. As the angle between the two mean directions (in the same hemisphere), $\gamma O=17.4^\circ$, is smaller than the critical angle $\gamma C=19.6^\circ$ at which the hypothesis of a common mean direction for the distribution would be rejected, the test is positive (“type C” results are those where $10^\circ < \gamma C \leq 20^\circ$). Hence, the hypothesis of a common mean direction may not be rejected at the 95-percent confidence level. The antipodal character of IT and HT mean directions do not favour any interpretation involving local deformation occurring between the two acquisition times.

We argue that the IT component recorded roughly the same magnetization event, but with the opposite polarity of the Earth's magnetic field and we interpret the antipodal misfit as due to (1) an overlap of the IT component with the two other components and (2) insufficient averaging of the secular variation due to the small sampling set. Because of the large uncertainty of the IT component, its direction will not be used in the arguments following in the next section.

The HT component has a flattening parameter of $F=17.6 \pm 7.7^\circ$ with respect to the expected direction. In declination, it coincides with the expected direction (at any time during the last 20 Ma).

The LT direction of SA has a direction of $D=340.2^\circ$, $I=49.2^\circ$ and has therefore the expected inclination ($F=0.0 \pm 4.2^\circ$) but is rotated about a vertical axis by $19.7 \pm 5.9^\circ$ in an anti-clockwise sense with respect to stable NW Africa.

Table 8

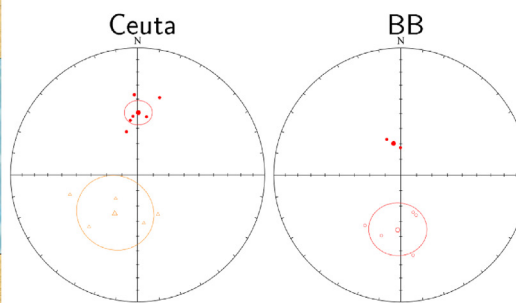
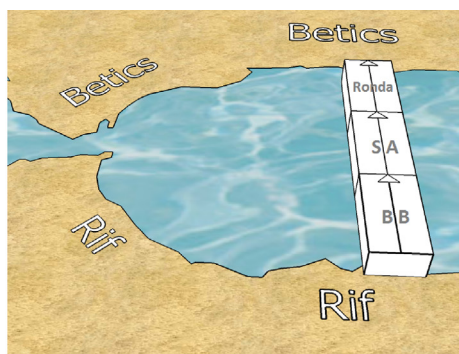
Atomic percentages of the elements from the EDX analyses of the SA samples.

Position	Sample	Fe	Mg	Si	O	Ni	Al	S	Cr	Co	Ca	Cu	Ti	Mn	Cl
1	BB5-6B	9.8	11.3	1.3	41.9		19.8		15.8		0.2				
2	BB5-6B	5.8	11.6		47.3		22.8		12.5						
3	BB5-6B	1.1	15.8	6.4	24.5	0.3	3.3							48.7	
4	BB5-6B	32.1					20.9								
5	BB5-6B	3.7	23.2	16.2	54.6	0.9									
6	BB5-6B	46.0	2.4	2.1	49.7										
7	BB5-6B	52.0	0.6		47.4										
8	BB5-6B	6.1	11.6		47.5		24.5		10.4						
9	BB5-6B	37.4	2.5		47.2	0.3	0.9		11.6						
10	BB4-2B	2.1	24.8	17.9	53.0	2.3									
11	BB4-2B	8.3	22.7	11.4	45.9	4.7		2.1		5.0					
12	BB4-2B	4.8	24.8	13.2	49.9	6.8		0.2		0.4					
13	SA2-3A	24.3			12.6	11.6	3.5	35.5						12.5	
14	SA2-3A	27.8				25.7		46.5							
15	SA2-3A	8.4	50.2	41.4	^a	^b	0.0								
16	SA2-3A	5.8	44.3	49.3	^a		0.6								
17	SA2-3A	26.1	0.7	0.5		27.5		45.3							
18	SA2-3A	26.3				28.2		45.5							
19	SA2-3A	94.4	1.2	1.8	^c		2.6		^b						
20	SA2-3A	82.8	6.6	4.1	^c		6.5		^b						
21	SA2-3A	55.3	25.9	18.3	^a		0.5								
22	SA2-3A	46.1	2.0	1.2	47.9	0.4	1.0	1.0	0.4						
23	SA2-3A	24.9		0.5		27.6		47.0							
24	SA2-3A	30.2	8.2	0.5	43.7		14.3		3.1						
25	SA8-3A	36.5	5.0	2.6	47.7		4.2		3.3						0.7
26	SA8-3A	13.0	0.6	0.8		31.5		53.6		0.4					
27	SA8-3A	17.5	9.1	9.7	43.0		3.5		14.1		1.6				1.6
28	SA8-3A	34.0		9.7	6.1	50.2									
29	SA8-3A	7.6	18.1	11.7	37.5	9.1		16.1							
30	SA8-3A	54.0		0.7	45.3										

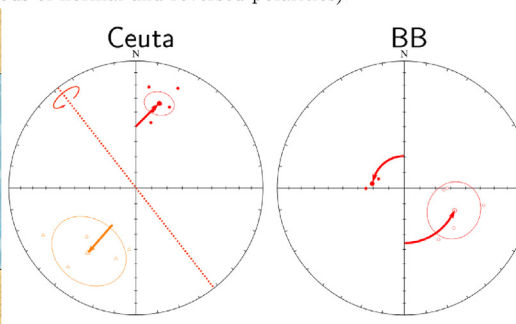
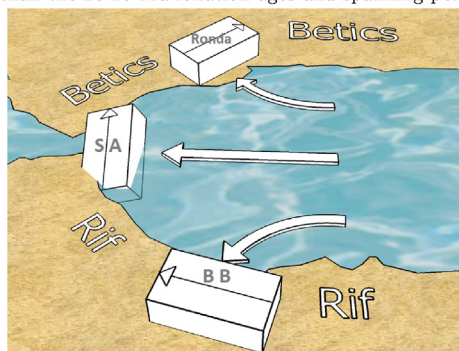
^a Oxygen present but the amount has not been calculated.

^b Small amount is possibly present but has not been calculated.

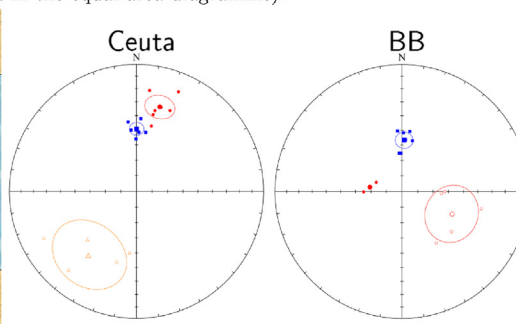
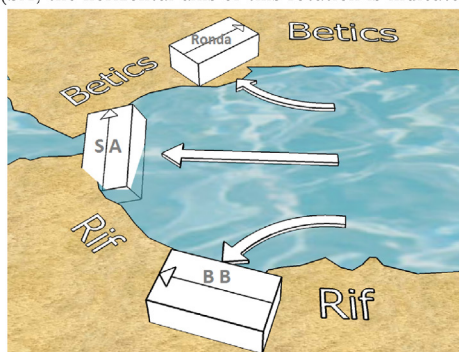
^c Presence or absence of oxygen unknown.



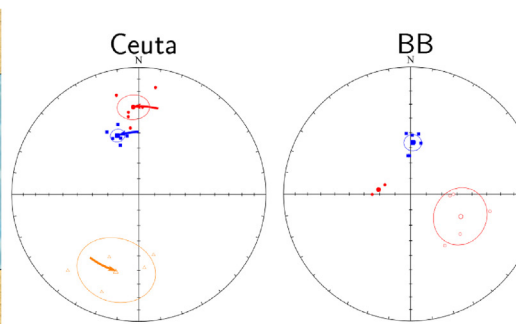
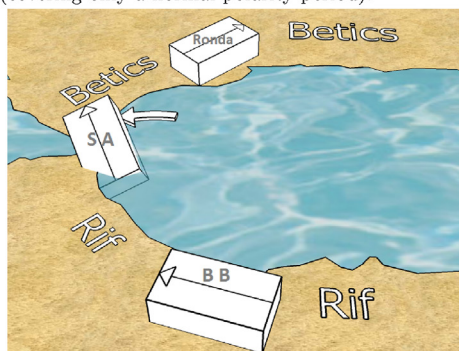
(a) Exhumation of the SA, BB and Ronda peridotites, followed by cooling, serpentinization, deformation, formation of SD magnetite grains and acquisition of a high and intermediate temperature CRM (younger than the 20–25 Ma foliation ages and spanning periods of normal and reversed polarities).



(b) Dismembering and large vertical-axis rotations (anticlockwise in BB and clockwise in Ronda) and tilt (SA, the horizontal axis of this rotation is indicated in the equal area diagramme).



(c) Another serpentinization, formation of MD magnetite grains and acquisition of a low temperature CRM (covering only a normal polarity period).



(d) Small anticlockwise rotation of SA. Note that the final stage corresponds with in situ observed directions.

Fig. 18. Schematic diagrams of the net rotations proposed for the Ceuta and Beni Bousera peridotites in successive stages. The boxes represent the Ceuta (SA), the Beni Bousera (BB) and the Ronda peridotites (note that the boxes do not indicate any accurate geographical location). The acquisition and in-situ rotations of the magnetic LT (blue squares), IT (yellow triangles) and HT (red circles) components. (For interpretation of the references to color in this figure legend, the reader is referred to the web version of this article.)

Table 9

Overview of the minerals that have been analyzed with their possible identification.

Position	Sample	Grain size	Major elements	Mineral
1	BB5-6B	10 µm	Fe, Mg, O, Al, Cr	Chromite ^a
2	BB5-6B	500 µm	Fe, Mg, O, Al, Cr	Chromite ^a
3	BB5-6B	10 µm	Cu, Mg, O	CuO+...
4	BB5-6B	50 µm	Fe, Ni, S	Pentlandite
5	BB5-6B	<1 µm	Mg, Si, O	Forsterite
6	BB5-6B	10 µm	Fe, O	Magnetite
7	BB5-6B	10 µm	Fe, O	Wüstite
8	BB5-6B	50 µm	Al, Mg, O, Cr	Pyroxene/chromite
9	BB5-6B	5 µm	Fe, O, Cr	Magnetite/chromite
10	BB4-2B	10 µm	Mg, Si, O	Forsterite
11	BB4-2B	1 µm	Mg, Si, O	Forsterite
12	BB4-2B	1 µm	Mg, Si, O	Forsterite
13	SA2-3A	100 µm	Fe, Ni, S, Cu, O	Pentlandite + CuO
14	SA2-3A	50 µm	Fe, Ni, S	Pentlandite
15	SA2-3A	100 µm	Fe, Mg, Si, O ^b	Pyroxene/olivine
16	SA2-3A	Matrix	Mg, Si, O ^b	Pyroxene/olivine
17	SA2-3A	10 µm	Fe, Ni, S	Pentlandite
18	SA2-3A	10 µm	Fe, Ni, S	Pentlandite
19	SA2-3A	10 µm	Fe, O ^c	Magnetite/hematite
20	SA2-3A	10 µm	Fe, O ^c	Magnetite/hematite
21	SA2-3A	10 µm	Fe, Mg, Si, O ^c	Olivine ^b
22	SA2-3A	5 µm	Fe, O	Wüstite
23	SA2-3A	10 µm	Fe, Ni, S	Pentlandite
24	SA2-3A	10 µm	Fe, O, Al	Magnetite/hematite ^a
25	SA8-3A	10 µm	Fe, O	Magnetite/hematite
26	SA8-3A	10 µm	Fe, Ni, S	Pentlandite
27	SA8-3A	10 µm	Fe, Mg, Si, O, Cr	Fayalite ^c
28	SA8-3A	5 µm	Fe, Mg, Si, O	Magnetite/hematite
29	SA8-3A	1 µm	Fe, Mg, Si, O, Ni, S	Pentlandite
30	SA8-3A	50 µm	Fe, O	Wüstite

^a See note of Table 8.^b Contains substantial amounts of Al.^c Contains substantial amounts of Fe.^c Contains substantial amounts of Cr.

7.5. Palaeomagnetic constraints on timing and geodynamic evolution

As described in Section 7.2, the IT (of SA) and HT (of BB and SA) components are likely due to the first serpentinization stage during the post-metamorphic cooling, after the deformation (foliation, folded pyroxenite veins) dated between 25 and 20 Ma ago, and after the BB (undated) age of folding. The LT components are likely due to a posterior serpentinization. Then, in Beni Bousera the older component (HT) is rotated, whilst the younger one (LT) is present-day north, and there is no tilt apparent in either component.

In SA, the older HT component points north but is tilted and the younger LT component is rotated about a vertical axis but has no tilt. As the HT and IT components are roughly antipodal, we argue that the IT and HT components were roughly recorded at the same time. Due to the similarities in mineralogy we also argue that the acquisition times roughly coincide between the respective components of SA and BB.

We therefore propose the following model of a relative sequence of events leading to the observed remanent magnetizations: after their exhumation and post-metamorphic cooling, both the Beni Bousera massif and the Sarchal massif (Ceuta) recorded a first magnetic component during a first serpentinization phase (Fig. 18(a)). During this time, at least one geomagnetic field reversal occurred that was recorded by both BB and SA. In SA, it is noteworthy that the reversed polarity directions have systematically lower unblocking temperatures. This may be explained if at some point during the first serpentinization the size distribution of the newly formed grains changed slightly. This would then imply that there occurred exactly one field reversal during the acquisition of remanence in SA, recording one polarity by one grain size distribution and the other polarity by another grain size distribution.

After the acquisition of the first remanence, the peridotites dismembered and BB rotated by $72.3 \pm 12.1^\circ$ (data from this work and Saddiqi et al. (1995)) in an anticlockwise direction about a vertical axis (Fig. 18(b)). Then, the BB peridotites recorded another magnetic component (LT), probably during the formation of larger magnetite grains during the posterior serpentinization. After that there were no further net rotations in the BB massif.

In order to explain the geodynamic evolution of the Ceuta peridotites with the least number of rotations possible, we first observe that the “young” LT component of SA describes a 19.8° anticlockwise rotation about a vertical axis with respect to the expected direction of stable NW Africa. By rotating the measured directions by an equal amount in the opposite direction, we find the magnetic directions of the peridotites as they must have been at the time of the acquisition of the young LT component. From there, by comparing both declination and inclination of the LT and the HT (assuming the IT component to be antipodal to HT), one finds that the older HT (and IT) component can be interpreted as a (pure) a tilt of 25° (with the south-west going downwards) about a horizontal axis with azimuth 145° with respect to the expected direction of stable NW Africa. Alternatively, one could choose different rotation axes up to a plunge of -50° to describe the rotation between the acquisition of the HT and the LT components. A rotation axis of plunge -50° would have an azimuth of 72° and a rotation about 30° (clockwise and south-east going downwards). The smallest possible rotation between the two components is a rotation of about 22° about an axis of azimuth ca. 115° and plunge ca. -30° (south going downwards).

Hence, after the acquisition of the HT and IT components, the SA massif tilted with the south moving downwards (Fig. 18(b)) at the same relative time when the rotation of BB took place. Then, the SA peridotites acquired the LT component during another serpentinization phase. Afterwards, they rotated $19.7 \pm 5.9^\circ$ about a vertical axis in an anti-clockwise fashion (Fig. 18(d)). Note that, even if the relatively small rotations in SA were disputed because of palaeosecular variation, small-scale tectonic deformations, etc., an important fact that future geodynamic models have to incorporate is that the SA peridotites did not experience any large vertical-axis rotations that the BB and Ronda peridotites experienced.

8. Conclusions

This study has obtained new data about the magnetic mineralogy and the remanences of the Rifean peridotites including for the first time those located in Ceuta. Very detailed thermal and AF demagnetization, rock magnetic and SEM experiments suggested different candidates of magnetic minerals but indicated that the magnetic remanences of the peridotites are mostly carried by magnetite. There exist two distinct grain size populations of magnetite: one in the SD/PSD range (sometimes with overlapping reversed and normal polarities) and one in the MD range (always normal polarity) that carry different directional components. Hence, contrary to earlier studies in BB, the mechanism of remanence acquisition of all the magnetic components in both the BB and SA peridotites is most likely a CRM (note that the serpentinization processes causing a CRM are beyond the scope of this palaeomagnetic study).

Integrating the results of the all the experiments, a sequence of geodynamic stages can be inferred (note that we cannot infer any longitudinal or latitudinal constraints paleomagnetically, but only rotations):

1. A first remanent magnetization, of both normal and reversed polarities, was acquired by the BB and SA peridotites by the formation of SD/PSD magnetite grains during a serpentinization phase after their exhumation and subsequent cooling

- (postdating high temperature deformation and the age of folding of the BB anticline) about 20 Ma ago.
2. After their dismembering, the Ceuta peridotites, unlike their BB and Ronda counterparts, were tilted by some 22–30°, south moving downwards. The Beni Bousera peridotites were rotated anticlockwise by $72.3 \pm 12.1^\circ$ about a vertical axis. The reliability of this rotation has been improved in this study by the first observation of normal polarity directions of the older HT component of BB. Moreover, whilst a TRM as the mechanism of remanence acquisition, as was suggested in earlier works, would imply a rapid rotation of BB that took only two consecutive subchrons and was completely finished by the end of the post-metamorphic cooling (16 Ma), our interpretation as a CRM favour a rotation *posterior* to the serpentization of the post-metamorphic cooling and does not require such a fast rotation.
 3. At a later stage, both SA and BB recorded another magnetic signal of normal polarity only, carried by multi-domain magnetite grains. This is the only timing constraint of the rotation of BB (contrary to the earlier TRM interpretation).
 4. Finally, the Ceuta peridotites rotated anticlockwise by $19.7 \pm 5.9^\circ$ about a vertical axis. It is noteworthy that this rotation was (1) much smaller than the rotations found in Beni Bousera and Ronda (see Section 1.3) and (2) have taken place at a later stage than those at the other sites (if one assumes that stage three is roughly coeval for the three bodies).
- The new palaeomagnetic data of the Ceuta and the Beni Bousera peridotites that have been found in this study are constraints that need to be incorporated in any geodynamic model of the evolution of the Betic–Rifean mountain belt.

Acknowledgements

We are thankful for the financial support from the Spanish projects PR27/05-13936-BSCH, CGL2009-10840, CGL2011-29474-C02-01 and CGL2012-38481. VCRM is especially grateful to his colleagues D. García, F.J. Pavón, G. McIntosh, V. Villasante and I. Palencia for their geological guidance and assistance during field-work. We would also like to express our gratitude to A. Crespo Blanc and M. Maffione, whose various comments have greatly improved this work.

Appendix A.

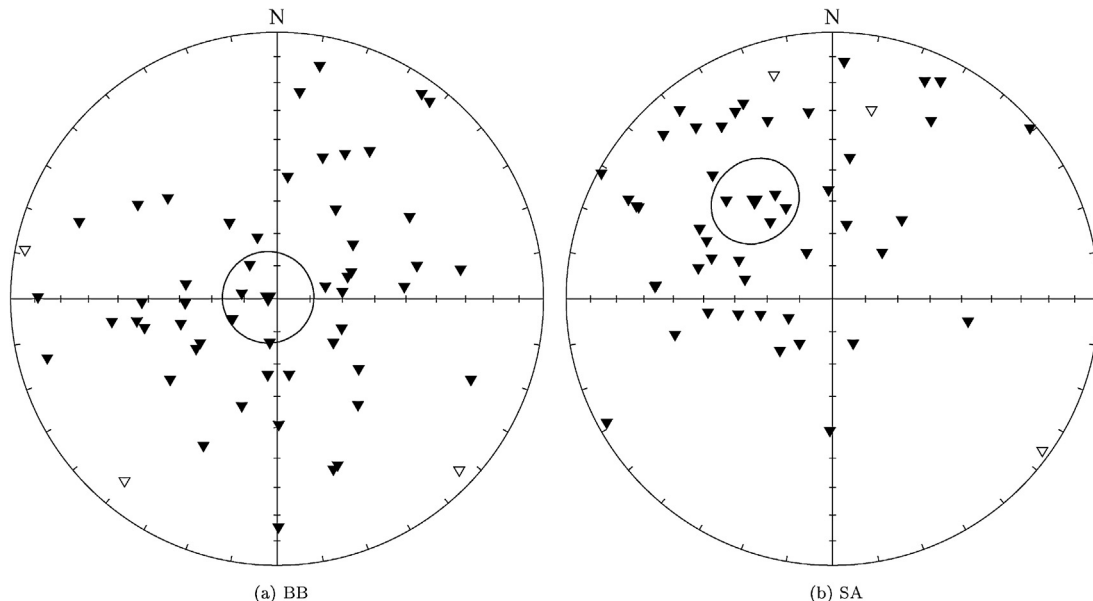


Fig. 19. Magnetic directions below 180°C (BB) and 100°C (SA). Mean directions and α_{95} confidence levels are indicated.

References

- Afifi, A., Gueydan, F., Pitra, P., Essaifi, A., Précigout, J., 2011. Oligo-miocene exhumation of the beni-bousera peridotite through a lithosphere-scale extensional shear zone. *Geodin. Acta* 24 (1), 49–60.
- Allerton, S., Lonergan, L., Platt, J., Platzman, E., McClelland, E., 1993. Palaeomagnetic rotations in the Eastern Betic Cordillera, Southern Spain. *Earth Planet. Sci. Lett.* 119 (3), 225–241.
- Andrieux, J., Fontbote, J.-M., Mattauer, M., 1971. Sur un modèle explicatif de l'arc de gibraltar. *Earth Planet. Sci. Lett.* 12 (2), 191–198.
- Balanyá, J., Garcí a-Due nas, V., 1987. Les directions structurales dans le domaine d'alborán de part et d'autre du détroit de gibraltar. *Comptes rendus de l'Académie des sciences, Série 2, Mécanique, Physique, Chimie, Sciences de l'univers. Sci. Terre* 304 (15), 929–932.
- Barberá, X., Cabrera, L., Gomis, E., Parés, J., 1996. Determinación del polo paleomagnético para el límite oligoceno-mioceno en la cuenca del ebro. *Geogaceta* 20 (5), 1014–1016.
- Calvo, M., Cuevas, J., Tubiža, J., 2001. Preliminary palaeomagnetic results on oligocene–early miocene mafic dykes from southern Spain. *Tectonophysics* 332 (3), 333–345.
- Calvo, M., Osete, M.L., Vegas, R., 1994. Palaeomagnetic rotations in opposite senses in southeastern Spain. *Geophys. Res. Lett.* 21 (9), 761–764.
- Calvo, M., Vegas, R., Osete, M.L., 1997. Palaeomagnetic results from upper Miocene and Pliocene rocks from the internal zone of the eastern Betic Cordilleras (southern Spain). *Tectonophysics* 277 (4), 271–283.
- Chalouan, A., Michard, A., 2004. The alpine Rif belt (Morocco): a case of mountain building in a subduction–subduction-transform fault triple junction. *Pure Appl. Geophys.* 161 (3), 489–519.
- Chalouan, A., Michard, A., El Kadiri, K., Negro, F., Frizon de Lamotte, D., Ji, S., Saddiqi, O., 2008. The Rif belt. In: Michard, A., Saddiqi, O., Chalouan, A., de Lamotte, D.F. (Eds.), *Continental Evolution: The Geology of Morocco: Structure, Stratigraphy, and Tectonics of the Africa–Atlantic–Mediterranean Triple Junction*. Springer Verlag Berlin Heidelberg.
- Cifelli, F., Mattei, M., Porreca, M., 2008. New paleomagnetic data from oligocene–upper Miocene sediments in the Rif chain (northern Morocco): insights on the Neogene tectonic evolution of the Gibraltar Arc. *J. Geophys. Res.: Solid Earth* (1978–2012) 113 (B2).
- Day, R., Fuller, M., Schmidt, V., 1977. Hysteresis properties of titanomagnetites: grain-size and compositional dependence. *Phys. Earth Planet. Inter.* 13 (4), 260–267.
- Deenen, M.H., Langereis, C.G., van Hinsbergen, D.J., Biggin, A.J., 2011. Geomagnetic secular variation and the statistics of palaeomagnetic directions. *Geophys. J. Int.* 186 (2), 509–520.
- Demarest, H.H., 1983. Error analysis for the determination of tectonic rotation from paleomagnetic data. *J. Geophys. Res.: Solid Earth* (1978–2012) 88 (B5), 4321–4328.
- Dunlop, D., Özdemir, Ö., 1997. *Rock Magnetism: Fundamentals and Frontiers. Cambridge Studies in Magnetism*. Cambridge University Press, Cambridge, United Kingdom.
- Dunlop, D., Özdemir, Ö., 2009. Magnetizations in rocks and minerals. In: Kono, M. (Ed.), *Geomagnetism: Treatise on Geophysics*. Elsevier, Amsterdam, Netherlands.
- Dunlop, D.J., 2002. Theory and application of the day plot (MRS/MS versus HCR/HC) 1. theoretical curves and tests using titanomagnetite data. *J. Geophys. Res.* 107 (B3), 2056.
- Dunlop, D.J., 2002. Theory and application of the day plot (MRS/MS versus HCR/HC) 2. application to data for rocks, sediments, and soils. *J. Geophys. Res.: Solid Earth* (1978–2012) 107 (B3), EPM-5.
- Feinberg, H., Saddiqi, O., Michard, A., 1996. New constraints on the bending of the Gibraltar arc from palaeomagnetism of the Ronda peridotites (Betic Cordilleras, Spain). *Geol. Soc. Lond. Special Publ.* 105 (1), 43–52.
- Fisher, R., 1953. Dispersion on a sphere. *Proc. R. Soc. Lond. Ser. A. Math. Phys. Sci.* 217 (1130), 295–305.
- Frizon de Lamotte, D., Andrieux, J., Guezou, J.-C., 1991. Cinématique des chevauchements néogènes dans l'arc Bético-Rifaïn; discussion sur les modèles géodynamiques. *Bull. Soc. Geol. France* 162 (4), 611–626.
- Gysi, A.P., Jagoutz, O., Schmidt, M.W., Targiusti, K., 2011. Petrogenesis of pyroxenites and melt infiltrations in the ultramafic complex of Beni Bousera, Northern Morocco. *J. Petrol.* 52 (9), 1679–1735.
- Halls, H.C., 1976. A least-squares method to find a remanence direction from converging remagnetization circles. *Geophys. J. R. Astronom. Soc.* 45 (2), 297–304, <http://dx.doi.org/10.1111/j.1365-246X.1976.tb00327.x>.
- Jasonov, P., Nourgaliev, D., Burov, B., Heller, F., 1998. A modernized coercivity spectrometer. *Geol. Carpath.* 49, 224–226.
- Kirschvink, J., 1980. The least-squares line and plane and the analysis of palaeomagnetic data. *Geophys. J. Int.* 62 (3), 699–718.
- Kornprobst, J., 1969. Le massif ultrabasique de Beni Bousera (Rif Interne, Maroc): étude des péridotites de haute température et de haute pression, et des pyroxénolites, à grenat ou sans grenat, qui leur sont associées. *Contrib. Mineral. Petrol.* 23, 283–322.
- Krijgsman, W., Garces, M., 2004. Palaeomagnetic constraints on the geodynamic evolution of the Gibraltar Arc. *Terra Nova* 16 (5), 281–287.
- Lonergan, L., White, N., 1997. Origin of the Betic–Rif mountain belt. *Tectonics* 16 (3), 504–522.
- Loomis, T., 1975. Tertiary mantle diapirism, orogeny and plate tectonics east of the strait of Gibraltar. *Am. J. Sci.* 275 (1), 1–30.
- Maffione, M., Morris, A., Plümper, O., van Hinsbergen, D.J., 2014. Magnetic properties of variably serpentized peridotites and their implication for the evolution of oceanic core complexes. *Geochem. Geophys. Geosyst.*
- Martin-Hernandez, F., Ferre, E., Belley, F., Ruiz-Martinez, V., Garrido, C., Osete, M., 2009. Magnetic signature and fabric of serpentized mantle rocks in the Betic–Rif arc and tectonic implications. In: *AGU Spring Meeting Abstracts*, vol. 1, p. 04.
- Mattei, M., Cifelli, F., Rojas, I.M., Crespo Blanc, A., Comas, M., Faccenna, C., Porreca, M., 2006. Neogene tectonic evolution of the Gibraltar Arc: new paleomagnetic constrains from the Betic chain. *Earth Planet. Sci. Lett.* 250 (3), 522–540.
- McFadden, P., McElhinny, M., 1990. Classification of the reversal test in palaeomagnetism. *Geophys. J. Int.* 103 (3), 725–729.
- Michard, A., Chalouan, A., Feinberg, H., Goffé, B., Montigny, R., 2002. How does the alpine belt end between Spain and Morocco? *Bull. Soc. Géol. France* 173 (1), 3–15.
- Michard, A., Chalouan, A., Montigny, R., Ouazzani-Touhami, M., 1983. Les nappes cristallophylliennes du Rif (sebtides, maroc), témoins d'un édifice alpin de type penninque incluant le manteau supérieur. *CR Acad. Sci. Ser. II* 296, 1337–1340.
- Michard, A., Goffé, B., Bouybaouene, M., Saddiqi, O., 1997. Late Hercynian–Mesozoic thinning in the Alboran domain: metamorphic data from the Northern Rif, Morocco. *Terra Nova* 9 (4), 171–174.
- Monié, P., Galindo-Zaldívar, J., Loderio, F., Goffé, B., Jabaloy, A., 1991. 40Ar/39Ar geochronology of alpine tectonism in the Betic Cordilleras (southern Spain). *J. Geol. Soc.* 148 (2), 289–297.
- Najid, D., Westphal, M., Hernandez, J., 1981. Paleomagnetism of quaternary and miocene lavas from north-east and central Morocco. *J. Geophys.* 49, 149–152.
- Osete, M., Freeman, R., Vegas, R., 1988. Preliminary palaeomagnetic results from the subbetic zone (Betic Cordillera, Southern Spain): kinematic and structural implications. *Phys. Earth Planet. Inter.* 52 (3), 283–300.
- Osete, M., Freeman, R., Vegas, R., 1989. Palaeomagnetic evidence for block rotations and distributed deformation of the Iberian–African plate boundary. In: *Paleomagnetic rotations and continental deformation*. Kluwer Academic Publishers, The Netherlands, pp. 381–391.
- Osete, M., Villalá n, J., Palencia, A., Osete, C., Sandoval, J., DUENAS, V.G., 2004. New palaeomagnetic data from the Betic Cordillera: constraints on the timing and the geographical distribution of tectonic rotations in southern Spain. In: *Geodynamics of Azores–Tunisia*. Springer, pp. 701–722.
- Platt, J., Vissers, R., 1989. Extensional collapse of thickened continental lithosphere: a working hypothesis for the Alboran Sea and Gibraltar Arc. *Geology* 17 (6), 540–543.
- Platt, J.P., Behr, W.M., Johanesen, K., Williams, J.R., 2013. The Betic–Rif Arc and its orogenic hinterland: a review. *Ann. Rev. Earth Planet. Sci.* 41, 313–357.
- Platzman, E., 1992. Paleomagnetic rotations and the kinematics of the Gibraltar Arc. *Geology* 20 (4), 311–314.
- Platzman, E., Lowrie, W., 1992. Paleomagnetic evidence for rotation of the Iberian Peninsula and the external Betic Cordillera, southern Spain. *Earth Planet. Sci. Lett.* 108 (1), 45–60.
- Platzman, E., Platt, J., Olivier, P., 1993. Palaeomagnetic rotations and fault kinematics in the Rif Arc of Morocco. *J. Geol. Soc.* 150 (4), 707–718.
- Reuber, I., Michard, A., Chalouan, A., Juteau, T., Jermoumi, B., 1982. Structure and emplacement of the alpine-type peridotites from Beni Bousera, Rif, Morocco: a polyphase tectonic interpretation. *Tectonophysics* 82 (3), 231–251.
- Rochette, P., Fillion, G., Mattéi, J.-L., Dekkers, M.J., 1990. Magnetic transition at 30–34 Kelvin in Pyrrhotite: insight into a widespread occurrence of this mineral in rocks. *Earth Planet. Sci. Lett.* 98 (3), 319–328.
- Saddiqi, O., Feinberg, H., El Azzab, D., Michard, A., 1995. Paléomagnétisme des péridotites des Beni Bousera (Rif Interne, Maroc): conséquences pour l'évolution miocène de l'arc de gibraltar. *C. R. Acad. Sci.* 321, 361–368.
- Sánchez-Gómez, M., Due nas, V.G., Mu noz, M., Balanyá, J.C., 1995. Relación estructural entre los cuerpos peridotíticos situados al norte y al sur del estrecho de gibraltar. *Geogaceta* 17 (17), 135–137.
- Sánchez-Rodríguez, L., Gebauer, D., 2000. Mesozoic formation of pyroxenites and gabbros in the Ronda area (southern Spain), followed by early miocene subduction metamorphism and emplacement into the middle crust: U–Pb sensitive high-resolution ion microprobe dating of zircon. *Tectonophysics* 316 (1), 19–44.
- Seidemann, D.E., 1976. An 40Ar/39Ar age spectrum for a cordierite-bearing rock: isolating the effects of excess radiogenic 40Ar. *Earth Planet. Sci. Lett.* 33 (2), 268–272.
- Torsvik, T.H., Van der Voo, R., Preeden, U., Mac Niocaill, C., Steinberger, B., Doubrovine, P.V., van Hinsbergen, D.J., Domeier, M., Gaina, C., Tohver, E., et al., 2012. *Phanerozoic polar wander, palaeogeography and dynamics*. Elsevier, Amsterdam, Netherlands.
- Villalá n, J., Osete, M., Vegas, R., Garcí a-Due nas, V., Heller, F., 1994. Widespread neogene remagnetization in jurassic limestones of the South-Iberian Palaeomargin (Western Betics, Gibraltar Arc). *Phys. Earth Planet. Inter.* 85 (1), 15–33.
- Villalá n, J., Osete, M., Vegas, R., Garcí a-Due nas, V., Heller, F., 1996. The neogene remagnetization in the western Betics: a brief comment on the reliability of palaeomagnetic directions. *Geol. Soc. Lond. Spec. Publ.* 105 (1), 33–41.
- Villasante-Marcos, V., Osete, M., Gerville, F., García-Duena, V., 2003. Palaeomagnetic study of the ronda peridotites (Betic Cordillera, Southern Spain). *Tectonophysics* 377 (1), 119–141.
- Zeck, H.P., Monié, P., Villa, I.M., Hansen, B.T., 1992. Very high rates of cooling and uplift in the alpine belt of the Betic Cordilleras, Southern Spain. *Geology* 20 (1), 79–82.